HHS Public Access

Author manuscript

*J Am Chem Soc*. Author manuscript; available in PMC 2017 September 14.

Published in final edited form as:

*J Am Chem Soc*. 2016 September 14; 138(36): 11410–11428. doi:10.1021/jacs.6b05251.

# Activation of Dioxygen by Iron and Manganese Complexes: A Heme and Nonheme Perspective

**Sumit Sahu**[†] and **David P. Goldberg**[†,*]

[†]Department of Chemistry, The Johns Hopkins University, Baltimore, Maryland 21218, United States

## Abstract

The rational design of well-defined, first-row transition metal complexes that can activate dioxygen has been a challenging goal for the synthetic inorganic chemist. The activation of $O_2$ is important in part because of its central role in the functioning of metalloenzymes, which utilize $O_2$ to perform a number of challenging reactions including the highly selective oxidation of various substrates. There is also great interest in utilizing $O_2$, an abundant and environmentally benign oxidant, in synthetic catalytic oxidation systems. This Perspective brings together recent examples of biomimetic Fe and Mn complexes that can activate $O_2$ in heme or nonheme-type ligand environments. The use of oxidants such as hypervalent iodine (e.g., ArIO), peracids (e.g., *m*-CPBA), peroxides (e.g., $H_2O_2$) or even superoxide is a popular choice for accessing well-characterized metal–superoxo, metal–peroxo, or metal–oxo species, but the instances of biomimetic Fe/Mn complexes that react with dioxygen to yield such observable metal–oxygen species are surprisingly few. This Perspective focuses on mononuclear Fe and Mn complexes that exhibit reactivity with $O_2$ and lead to spectroscopically observable metal–oxygen species, and/or oxidize biologically relevant substrates. Analysis of these examples reveals that solvent, spin state, redox potential, external co-reductants, and ligand architecture can all play important roles in the $O_2$ activation process.

## 1. INTRODUCTION

Dioxygen, arguably the most important molecule for sustaining aerobic life, plays a number of critical roles in biology, ranging from nutrient metabolism to the synthesis of various important biomolecules (e.g., aromatic amino acids, hormones, neuro-transmitters).[1] Most of these processes rely on the oxidizing power of dioxygen, where it undergoes four-electron reduction to form water. This four-electron reductive activation of dioxygen, although thermodynamically favorable overall (0.815 V vs NHE in water at pH 7, 25 °C), is kinetically hindered, because the dioxygen molecule is found in a triplet spin ground state and has a high negative one-electron reduction potential (−0.33 V vs NHE in water at pH 7, 25 °C).[2] Nature can overcome the spin state barrier by employing transition metal ions that also exist in open-shell spin ground states and can react directly with triplet dioxygen. These metal ions can facilitate the one-electron reduction of $O_2$ by metal coordination, and also can

[*]**Corresponding Author** dpg@jhu.edu.

The authors declare no competing financial interest.

serve as multielectron reductants to access thermodynamically more favorable two-electron, or even four-electron reduction pathways. A number of first-row transition metals ions (such as Mn, Fe, Cu) are employed by metalloenzymes for the purpose of activating $O_2$, and the power and breadth of these enzymes have captured the imagination of biochemists, inorganic chemists, and other researchers for many years.

Iron-containing enzymes make up a large number of these $O_2$-activating enzymes, partly because of the bioavailability of iron in Nature, and partly because iron can access multiple redox states. In addition, there are a number of open-shell spin states available to iron in its different common oxidation states, with high-spin (hs) iron(II) ($S = 2$) perhaps being the most important with regard to the binding and activation of $O_2$. The Fe-containing enzymes can be classified into two types: heme enzymes, which contain a macrocyclic porphyrinoid ligand which houses the metal center, and nonheme iron enzymes, which have nonporphyrinoid ligand coordination (e.g., two-histidine-1-carboxylate binding motif) holding the iron ion in the protein. Both heme[3–5] and nonheme[1,6,7] Fe enzymes reductively activate $O_2$ in their respective catalytic cycles, and often target the oxidation of organic substrates, including aliphatic C–H hydroxylation, aromatic hydroxylation, olefin epoxidation, and halogenation reactions. Although heme and nonheme enzymes have very different structural features, they share similar iron–oxygen intermediates (e.g., iron–superoxo, iron–(hydro)peroxo, high-valent iron–oxo) during their respective catalytic cycles. Spectroscopic evidence for some of these intermediates has been obtained,[8] but trapping these intermediates, and studying their spectroscopic and reactivity properties inside the protein scaffold remains quite challenging because of their short lifetimes, general instability, and the inherent difficulties in studying large macromolecular complexes.

Synthetic biomimetic model complexes have been prepared and their reactivity has been studied over the years to aid in the understanding of these biological processes. The mechanisms and key intermediates involved are often more easily studied in these small-molecule analogue systems. Heme and nonheme iron complexes have received a great deal of attention because of their relevance to biology, and much effort has gone into their synthetic development and the study of their rich spectroscopic features as well as their reactivity. Mn-based complexes have gathered increasing attention as a close analogue of Fe-based systems, owing to the fact that both Fe and Mn share similar coordination geometries and multiple redox states, and also because of Mn sites in biology (e.g., photosystem II, superoxide dismutase, ribonucleotide reductase, Mn catalases).[9,10] Although the direct reactivity of Fe and Mn complexes with dioxygen has led only to limited progress, some progress has been made by studying organic and inorganic oxidants (PhIO, *m*-CPBA, $H_2O_2$, NaOCl, ROOH) as surrogates for $O_2$ and as tools for accessing proposed $O_2$-derived intermediates. A number of review articles have been written describing this chemistry for both heme and nonheme model complexes.[6,8,10–19]

In this Perspective, we present recent, significant findings on the activation of $O_2$ by mononuclear iron and manganese complexes. As opposed to earlier reviews, we focus exclusively on reactivity with dioxygen as the oxidant, and we bring together both heme and nonheme systems for comparison. We also attempt to provide a brief description of the structural and electronic factors that help facilitate and control the binding and activation of

dioxygen at the different metal sites. This Perspective separately considers heme and nonheme systems as a convenient way to categorize and discuss the progress that has been made in these areas over the past 10 years.

## 2. DIOXYGEN REACTIVITY OF IRON-PORPHYRIN COMPLEXES

Heme proteins are ubiquitous in nature and they perform a diverse range of biological functions including dioxygen transportation (e.g., hemoglobin) and storage (e.g., myoglobin), electron transfer (e.g., cytochrome c oxidase) and various organic transformations (mono and dioxygenases).[20] Heme proteins employ a planar, tetradentate porphyrin macrocycle as the ligand for the iron center. The iron porphyrin cofactor typically is coordinated to the protein by one or two axial ligand(s) with N, S, or O donor atoms (e.g, histidine, cysteine, methionine, tyrosine), and these ligands play an important role in controlling the reactivity at the iron center.[3,4] Cytochrome P450 (CYP) is one such enzyme and is the prototype of a dioxygen activating heme enzyme. The resting state of the CYP active site contains a ferric center with a cysteinate ligand in the axial position, which facilitates the dioxygen activation process at the iron center. The Cytochromes P450 carry out many chemical transformations, including the regioselective hydroxylation of challenging organic C–H substrates. The CYP enzymes utilize NADH as a source of reducing equivalents, and together with dioxygen give an $Fe^{IV}(O)$ π-cation-radical species (Compound I (Cpd-I)) that is capable of activating inert C–H bonds.

An early synthetic analogue for Cpd-I was prepared in 1979 with $[Fe^{III}(TPP)Cl]$ (TPP = *meso*-tetraphenylporphyrin) as the precursor complex.[21] However, an organic oxidant (PhIO, *m*-CPBA) was needed to generate this species, and most of the work on Cpd-I analogues that has followed since then still relies on the use of similar, high-energy oxidants.[21–23] Although efforts have been made to utilize $O_2$ to generate and characterize Cpd-I and other related $Fe/O_2$–derived intermediates during $O_2$ activation, successful examples of such chemistry remain limited. Challenges in forming Cpd-I from $O_2$ and synthetic porphyrins come from the difficulties in biasing synthetic systems toward favorable binding of $O_2$, and in providing the appropriate stoichiometry and timing of electrons and protons that must be added to achieve the multielectron cleavage of the O–O bond from $Fe^{II}$- or $Fe^{III}$-heme and $O_2$. Heme proteins such as P450 have a considerable advantage in carrying out this operation through evolutionarily optimized $e^-$ and $H^+$ transfer chains that guide the injection of reducing equivalents from NADH and $H^+$ from $H_2O$ into the active site heme iron. However, progress has been made in overcoming these obstacles, and some of these results are summarized in the following discussion.

From the 1960s, ferrous porphyrin complexes were known to bind and react with dioxygen to form the μ-oxo-bridged diiron(III) product.[24,25] The mechanism for this autoxidation was not fully understood until the 1980s, when the reaction was shown to proceed through a peroxo-bridged diiron(III) and the ferryl $Fe^{IV}(O)$ intermediates (Scheme 1).[26–29] Both the peroxo and oxo intermediates were characterized at low temperatures. Since that time, there have been relatively few studies describing the characterization of mononuclear, $O_2$-derived intermediates. There are few examples where an iron–porphyrin complex was shown to mediate substrate hydroxylation/epoxidation reactions utilizing dioxygen.[22,30–32] Some of

these systems required the use of an external reductant to observe the activity. Although a high-valent iron–oxo species was postulated as the active oxidant in most of these cases, there was very little spectroscopic evidence for the proposed oxidant, and the mechanism of the catalytic transformations were also poorly understood. The instability of these species makes their isolation and characterization quite challenging, and in the next section we highlight some of the recent examples in this area, where iron–oxygen species have been characterized. It is important to note that a large amount of work has been done on iron–porphyrin-based electrocatalysts for the reduction of oxygen;[33–38] however, these systems will not be covered in this Perspective.

Most of the dioxygen activating heme and nonheme iron enzymes are proposed to proceed through an initially formed iron(III)–superoxide intermediate. In synthetic heme systems, formation of an $Fe^{III}(O_2^-)$ complex was reported for a few cases.[39–41] A later example of a porphyrinoid $Fe^{III}(O_2^-)$ species was reported in 2009 with [FeII(tmpIm)] as starting material (Scheme 2).[42] Reaction of [$Fe^{II}$(tmpIm)] with $O_2$ at −75 °C led to the formation of [$Fe^{III}(O_2^-)$(tmpIm)], which gave a characteristic UV–vis spectrum (426, 535, 589 nm). Stoichiometric addition of the one-electron reductant cobaltocene to the $Fe^{III}(O_2^-)$ species with excess MeOH generated the $Fe^{III}$(OOH) complex (427, 534, 564 and 610 nm). This result indicated that MeOH protonates an initially formed peroxo complex. Attempts to isolate the unprotonated peroxo species from dioxygen were unsuccessful. Interestingly, the same $Fe^{III}$(OOH) species could be produced by reacting [$Fe^{II}$(tmpIm)] with $KO_2$ and subsequent treatment with MeOH (Scheme 2). The formation of an $Fe^{III}$(OOH) species was confirmed by resonance Raman (rR) spectroscopy ($\nu_{O-O}$ = 810; $\nu_{Fe-O}$ = 570 $cm^{-1}$) and isotope labeling experiments with $^{18}O_2$ and MeOD. Zero-field Mössbauer and electron paramagnetic resonance (EPR) experiments revealed the presence of a low-spin (ls) $Fe^{3+}$ center in the hydroperoxide complex. Introduction of a bulky xanthene substituent on a *meso*-carbon atom of the tmpIm macrocycle led to stabilization of the unprotonated peroxo species.[43] The xanthene moiety was thought to provide steric shielding for the peroxo group. Reaction of the new xanthene appended [$Fe^{II}$(tmpIm)] complex with $O_2$ at −30 °C generated the $Fe^{III}(O_2^-)$ species, which was characterized by UV–vis (428, 550, 592 nm) and rR spectroscopy ($\nu_{Fe-O2}$ = 582 $cm^{-1}$). Addition of cobaltocene to the $Fe^{III}(O_2^-)$ species resulted in the formation of a ls-$Fe^{III}$-(peroxo) complex. This complex was characterized by UV–vis (430, 568, 610 nm), EPR ($g$ = 2.27, 2.16, 1.96), and rR spectroscopy ($\nu_{Fe-O}$ = 585 $cm^{-1}$, $\nu_{O-O}$ = 808 $cm^{-1}$). Based on the available spectroscopic data, an end-on $Fe^{III}$-(peroxo) species was proposed for the product from $Cp_2Co$ reduction.[43] In 2016, the same group showed that a related imidazole-ligated, ferrous–porphyrin complex with a pendant anthrace-necarboxylic acid group reacts with $O_2$ to give the $Fe^{III}(O_2^-)$ complex, and also yields the one-electron-reduced hydroperoxo complex with the $Fe^{II}$ starting porphyrin serving as reductant.[44]

The former work highlights the power of ligand design in improving the reactivity of these heme analogues. Tethering of the axial ligand to the synthetic porphyrin helps with facilitating $O_2$ binding and increasing the stability of the $O_2$ intermediates such that electrons and protons can be delivered. Further work on modifying axial ligation through ligand design may improve the $O_2$ activation chemistry in synthetic systems. The addition of second-coordination-sphere groups orthogonal to the plane of the porphyrin, such as the

pendant anthracene carboxylic acid described above, is another promising strategy for building discrete molecules with improved $O_2$ activation properties. These strategies, however, necessarily involve multistep organic synthesis, which can be a drawback. Other promising strategies may be to imbed and sequester porphyrins in modifiable, three-dimensional frameworks that can be readily synthesized, such as metal–organic frameworks (MOFs). A study was recently reported that led to the binding of $O_2$ to an iron porphyrin encapsulated in the MOF PCN-224$Fe^{II}$.[45] The encapsulation led to the trapping of a novel Fe–$O_2$ adduct that lacked a sixth axial ligand trans to the $O_2$ binding site.

## 3. MANGANESE–PORPHYRINOID COMPLEXES AND DIOXYGEN ACTIVATION

Manganese porphyrinoid complexes have been synthesized and examined for comparisons with the analogous iron complexes in heme enzymes. One of the early examples of dioxygen activation by a Mn–porphyrin complex was reported in 1975.[46] A side-on $Mn^{IV}$–peroxo species was proposed to form from the reaction of [$Mn^{II}$(TPP)(Py)] complex (Py = pyridine) with dioxygen at −78 °C.[47,48] A few other reports followed which described dioxygen reactivity of other Mn–porphyrin and Mn-phthalocyanine complexes.[49–53] Mn porphyrinoid complexes have also been used for substrate oxidations utilizing $O_2$ as the oxidant.[54,55] For example, one of the early examples of the use of $O_2$ as oxidant was reported in 1987, where [Mn(TPP)(Cl)] was reacted with $O_2$ in the presence of 1-methyl imidazole as cocatalyst and Zn as reducing agent for the epoxidation of olefins.[54] In most of these earlier studies, the characterization of the proposed metal–oxygen intermediates was not extensive, and the nature of the active oxidant species in substrate oxidation reactions was poorly understood. There were very few reports in which well-characterized porphyrinoid Mn–oxygen intermediates were generated from dioxygen. Recently, our group reported the generation of a high-valent $Mn^{V}$(O) porphyrinoid complex from a $Mn^{III}$–corrolazine and $O_2$. The catalytic oxidation of certain organic C–H substrates was achieved with this system.[56–58]

Corrolazine (Cz) is a ring-contracted member of the porphyrinoid family with a 3– charge when fully deprotonated, and was designed by our group to stabilize high-valent metal complexes. It has been used to generate stable high-valent metal–oxo complexes of iron, vanadium, chromium, rhenium, and manganese.[14,59] In the case of Mn, the high-valent [($TBP_8$Cz)$Mn^{V}$(O)] ($TBP_8$Cz = octakis(*p-tert*-butylphenyl)-corrolazinato$^{3-}$) was isolated and characterized at room temperature. This complex was initially prepared from the reaction of a $Mn^{III}$ precursor [($TBP_8$Cz)$Mn^{III}$] with the hypervalent iodine reagent PhIO. However, it was shown in 2012 that [($TBP_8$Cz)$Mn^{V}$(O)] could be synthesized from reaction of [($TBP_8$Cz)$Mn^{III}$] with $O_2$ as the oxidant in the presence of visible light (Scheme 3).[58]

Photoirradiation of [($TBP_8$Cz)$Mn^{III}$] ($\lambda_{max}$ = 432, 687 nm) with a white light source under ambient conditions in cyclohexane led to the formation of dark green [($TBP_8$Cz)-$Mn^{V}$(O)] ($\lambda_{max}$ = 419, 639 nm) (Scheme 3). The production of [($TBP_8$Cz)$Mn^{V}$(O)] was confirmed by $^1$H NMR spectroscopy and laser desorption/ionization mass spectrometry (LDI-MS). Control experiments showed that the presence of both visible light and air was required for the conversion of $Mn^{III}$ to $Mn^{V}$(O) corrolazine. Isotope labeling experiments with $^{18}O_2$

confirmed dioxygen as the source of the O-atom in the $Mn^{V}(O)$ product. It was proposed that the light-driven, aerobic oxidation of $Mn^{III}$ to $Mn^{V}(O)$ in cyclohexane involved the participation of solvent as a sacrificial reductant. This hypothesis was corroborated by the fact that the $Mn^{V}(O)$ complex was not formed when the solvent was changed to benzonitrile.[60] However, addition of toluene derivatives with relatively weak benzylic C–H bonds (e.g., hexamethylbenzene, HMB) resulted in the formation of $[(TBP_8Cz)Mn^{V}(O)]$ in PhCN (Scheme 3).[60] GC-MS analysis of the reaction with HMB revealed the production of pentamethylbenzyl alcohol in good yield (87%), together with a small amount of pentamethylbenzaldehyde (8%). A primary kinetic isotope effect (KIE) for the substrates toluene (KIE = 5.4) and mesitylene (KIE = 5.3) was observed, indicating that the initial cleavage of the benzylic C–H bond was involved in the rate-determining step. It was shown that this strategy could be expanded to manganese porphyrin complexes, where the catalytic aerobic oxidation of an activated substrate (acridine) was performed with air, visible light, and $Mn^{III}(Porph)(X)$ (X = OH, OAc).[61]

Further mechanistic insights came from femtosecond transient absorption spectroscopy.[60] The $[(TBP_8Cz)Mn^{III}]$ complex has a singquintet ($^5S_0$) ground state, due to high-spin $d^4$ electronic configuration. Femtosecond laser excitation of $[(TBP_8Cz)Mn^{III}]$ converted the singquintet ($^5S_0$) ground state to a tripquintet ($^5T_1$) excited state at 530 nm (Figure 1). This state undergoes rapid intersystem crossing to a long-lived tripseptet ($^7T_1$) state with a new peak at 774 nm (Figure 1). The decay rate of the $^7T_1$ state was sensitive to the presence of $O_2$. It was suggested that the $^7T_1$ state reacts directly with $O_2$ to form a $Mn^{IV}$–superoxo intermediate, which abstracts a H-atom from the toluene derivative to form a $Mn^{IV}(OOH)$ complex and benzyl radical. This latter step would be the rate-determining step based on KIEs. The subsequent breaking of the O–O bond could go through either a homolytic or heterolytic pathway, leading to the formation of $[(TBP_8Cz)\text{-}Mn^{V}(O)]$ and benzyl alcohol, as shown in Scheme 3.

The $[(TBP_8Cz)Mn^{V}(O)]$ complex can oxidize substrates with relatively weak C–H bonds such as dihydroacridine ($AcrH_2$, bond dissociation free energy (BDFE) = 69 kcal/mol) to give acridone (Acr═O), or O-atom acceptor substrates such as triphenylphosphine to give triphenylphosphine oxide.[58,60] These substrates allow for catalytic turnover with $Mn^{III}$ as catalyst in the presence of air and light (turnover number (TON) for ($OPPh_3$) = 535; TON(Acr═O) = 11). In a subsequent study, we hypothesized that strong acid would activate the photochemically generated $Mn^{V}(O)$ complex toward stronger C–H bonds (e.g., toluene (BDFE = 87 kcal $mol^{-1}$) and its derivatives), giving back the $Mn^{III}$ complex and completing a catalytic cycle.[11,56,57] Photoirradiation ($\lambda_{irr}$ > 400 nm) of a catalytic amount of $[(TBP_8Cz)Mn^{III}]$ in the presence of excess HMB and a strong proton donor $[H(OEt_2)2]^{+}[B\text{-}(C_6F_5)_4]^{-}$ ($H^{+}[B(C_6F_5)_4]^{-}$) in benzene resulted in the catalytic formation of oxidized alcohol PMB–OH and aldehyde PMB-CHO products in 18 and 9 turnovers, respectively. Although the TONs were modest, catalytic reactivity was achieved, and importantly, the resting state of the catalyst was shown to be $Mn^{III}$, with no evident buildup of the stable $Mn^{V}(O)$ complex under acidic conditions. The nature of the catalytically active species under acidic conditions was examined by spectroscopic methods and single-crystal X-ray diffraction (XRD). The corrolazine ligand contains *meso*-nitrogen atoms that are possible sites for protonation, and both the monoprotonated $[Mn^{III}(TBP_8CzH)]^{+}$ and diprotonated

$[Mn^{III}(TBP_8CzH_2)]^{2+}$ complexes were isolated and characterized by UV–vis. The structures of these complexes, together with the neutral $[Mn^{III}(TBP_8Cz)]$ were definitively proven by XRD.[57] It was found that monoprotonated $Mn^{III}(TBP_8CzH)^+$ was the catalytic resting state, as seen by UV–vis analysis of the catalytic reaction mixtures. The diprotonated complex was found to be catalytically unreactive. However, it was noted that a second equivalent of $H^+$ was necessary for catalytic turnover. The $Mn^{III}$ complex was not protonated by this second equivalent, but the second $H^+$ instead helped activate the transient Mn–oxo species for further reaction with substrate and subsequent closure of the catalytic cycle (Scheme 4).

In another study in 2016, the scope of the acid was also broadened to triflic acid, which led to a dramatic increase in catalytic turnover for the oxidations of HMB (TON = 563).[56] In addition, the same system was shown to carry out the catalytic oxidation of the sulfur substrate thioanisole, giving the corresponding sulfoxide with high turnover (TON = 902). As in the case of HBArF, the relevant mono- and diprotonated species were crystallographically characterized, and once again it was found that the monoprotonated complex was the catalytic resting state. Interestingly, the triflate anion was coordinated to $Mn^{III}$, and it was suggested that coordination of this counterion throughout the catalytic cycle (Scheme 4) may be responsible for the increase in catalytic activity.[56]

It remains to be seen if the photochemical activation seen for $Mn^{III}$ corrolazine can be extended to other metals, including iron. The analogous $Fe^{III}$ corrolazines are known, although the equivalent $Fe^{V}(O)$ corrolazine (characterized as $Fe^{IV}(O)$-$(Cz^{+\bullet})$) is much less thermally stable than the $Mn^{V}(O)$ complex.[62,63] Thus, the study of the photochemical/$O_2$ activation pathway will be more challenging in the analysis of the desired Fe–oxo complex. The closely related $Mn^{III}$ and $Fe^{III}$ corroles are also interesting future candidates for testing with $O_2$ and light.[64–67] These methods might lead to new corrole-derived high-valent metal–oxo species and/or catalytic oxidations.

The studies of the Mn porphyrinoid compounds described above are useful for comparison with the closely related iron systems. Examining the propensity to bind $O_2$ and the requirements for stabilizing high-valent metal–oxo species in Mn yields information that may be relevant to the analogous Fe systems, and provides continued motivation to study the Mn systems. There are also, of course, the Mn-containing biological systems pointed out in the Introduction that interact with and process dioxygen species. In addition, employing Mn porphyrinoid compounds as catalysts for the selective oxidation of organic compounds with $O_2$ as the oxidant remains an attractive, major goal in catalysis from an economic and environmental standpoint.

## 4. DIOXYGEN ACTIVATION BY NONHEME IRON COMPLEXES

Dioxygen activating nonheme iron enzymes are instrumental in a number of key biological processes such as synthesis of antibiotics and other biomolecules, DNA repair, and bio-degradation of aromatic compounds.[1,68] Most of these enzymes employ a two histidine and one carboxylate binding motif for the iron center coordination, while solvent molecules occupy the rest of the coordination sites. This 2-his-1-carboxylate binding motif exerts a weak ligand field, which is reflected in the high spin state for the ferrous center. However,

there are a number of enzymes (for example, cysteine dioxygenase) that have different coordinating ligands other than the 2-his-1-carboxylate triad. Although the majority of nonheme iron enzymes share similar ligand coordination, they can be classified into several categories (as shown in Figure 2), based on the identity of the cofactors and the functions they perform.[1,69] For example, extradiol cleaving catechol dioxygenase performs a C–C bond cleavage reaction of a catechol substrate, Rieske dioxygenase acts on an aromatic substrate to carry out a *cis*-dihydroxylation reaction, and pterin-dependent aromatic amino acid hydroxylases hydroxylate aromatic amino acid side chains. Similar to heme enzymes, various Fe–oxygen intermediates (such as superoxo, peroxo, oxo) were proposed in the catalytic cycles for nonheme iron enzymes. Few of them were characterized spectroscopically.[8] Model complexes provide important tools for detailed studies that are aimed at understanding the nature and reactivity of such iron–oxygen species in nonheme environments.

Biomimetic studies involving nonheme iron model complexes have received significant attention over the past 20 years with the advent of structural and spectroscopic data for a number of nonheme enzymes.[69] A range of polydentate ligands with different combinations of both nitrogen and oxygen donors were designed to model different features of enzyme active sites and led to a large class of nonheme iron complexes that were used to study reactivity and generate a number of biologically relevant “Fe–oxygen” intermediates (e.g., hydro-peroxo–, peroxo–, and oxo–iron species). A number of review articles have summarized the work in this area.[6,8,12,19] A major part of this nonheme iron chemistry, especially in the earlier efforts, relied on the use of external oxidants such as PhIO, *m*-CPBA and other peracids, $H_2O_2$ and tBOOH, instead of utilizing dioxygen as the oxidant and/or O-atom source. There were only a few examples of nonheme Fe complexes reacting with $O_2$ for substrate oxidation reactions.[6]

The activation of $O_2$ by synthetic nonheme iron complexes generally follows two possible pathways as shown in Scheme 5. The initial step involves coordination of $O_2$ to an $Fe^{II}$ center together with charge transfer to give a ferric–superoxo species. Addition of a proton/electron source can lead to further activation of the $O_2$ adduct, producing a (hydro)peroxo–iron(III) complex (pathway A, Scheme 5). For those studies involving O–O cleavage, mechanistic details are unclear in many cases, and both homolytic and heterolytic pathways are proposed. The final metal-bound iron–oxygen species is usually an $Fe^{IV}(O)$ species. Alternatively, a second iron(II) complex can take the place of the $H^+/e^-$ source, leading to the peroxo-bridged dinuclear species in pathway B. Homolytic cleavage of this intermediate gives the same terminal $Fe^{IV}(O)$ species as in pathway A. The high-valent $Fe^{IV}(O)$ intermediate acts as a potent oxidant in performing substrate oxidation reactions. In this section we describe some exciting, recent examples of nonheme iron mediated $O_2$ activation with a focus on the mechanism and the key intermediates as implied in Scheme 5.

### 4.1. Iron(III)–Superoxide

An $Fe^{III}(O_2^-)$ species is often proposed as the first intermediate in the catalytic cycle of nonheme iron enzymes that activate dioxygen. However, characterizing the superoxo species in the enzymatic systems has proven to be a difficult task and no such intermediate has been

observed for mononuclear nonheme Fe enzymes, although one example has been characterized in the diiron enzyme MIOX.[70] With the exception of iron, a number of metal–superoxo species in biomimetic systems have been characterized with a range of first-row transition metal ions (e.g., Cu, Cr, Ni). In some cases, the stability of the metal– superoxo species has lent itself to characterization by X-ray crystallography.[71–75] However, stabilizing a superoxo moiety derived from $O_2$ at a nonheme iron center has proven particularly difficult. The earliest report of a well characterized nonheme iron(III)–superoxide species involved a dinuclear iron complex and was reported in 2005.[76] This species was generated from a reaction of the dinuclear complex $[Fe_2(\mu\text{-}OH)_2(6\text{-}Me_3\text{-}TPA)_2](OTf)_2$ with $O_2$ at −80 °C, resulting in an "end-on" or $\eta^1$ $Fe^{III}$–$O_2^-$ intermediate ($\lambda_{max}$ = 325 nm (10 300 $M^{-1}$ $cm^{-1}$), 500 nm (1400 $M^{-1}$ $cm^{-1}$), 620 nm (1200 $M^{-1}$ $cm^{-1}$)). The nature of the dioxygen adduct was characterized as a superoxo ligand by rR spectroscopy ($\nu_{O–O}$ = 1310 $cm^{-1}$).

Despite much effort aimed at examining the reactivity between mononuclear iron complexes and $O_2$, it was not until 2014 that a mononuclear $Fe^{III}$ ($O_2^-$) complex was described (Scheme 6).[77] A doubly deprotonated BDPP ligand ($H_2$BDPP = 2,6-bis (((*S*)-2-(diphenylhydroxymethyl)-1-pyrrolidinyl)-methyl)pyridine) with a sterically encumbered bis(alkoxide) binding motif was used to promote $O_2$ activation and subsequent stabilization of the $Fe^{III}$ center. The red, square-pyramidal $Fe^{II}$ complex [$Fe^{II}$(BDDP)] was reacted with dioxygen in THF at −80 °C to give a bright yellow superoxide species [$Fe^{III}(O_2^-)$(BDDP)] ($\lambda_{max}$ = 330 nm, $\varepsilon$ = 9400 $M^{-1}$ $cm^{-1}$). The formation of this $O_2$ adduct was reversible, as sparging the solution with $N_2$ at −80 °C regenerated the $Fe^{II}$ precursor. The key identification of the superoxo moiety comes from rR spectroscopy on a frozen solution at 77 K ($\lambda_{ex}$ = 413.1 nm), which revealed a resonance-enhanced vibration at 1125 $cm^{-1}$. The energy of this vibration falls in line with other mononuclear metal–superoxide complexes ($\nu_{O–O}$ = 1100–1200 $cm^{-1}$).[71–74] Mössbauer spectroscopy of [$Fe^{III}(O_2^-)$-(BDDP)] revealed an isomer shift ($\delta$ = 0.58(3) mm/s) and hyperfine splitting pattern which was consistent with a hs-$Fe^{III}$ ($S$ = 5/2) center. An analysis of the Mössbauer data suggested a ferromagnetic spin-coupling interaction between the $Fe^{III}$ and $O_2^-$ ligand, which would result in an $S$ = 3 ground state.[78] The reactivity of [$Fe^{III}(O_2^-)$(BDDP)] toward H-atom abstraction was examined.[77] Treatment of the $Fe^{III}(O_2^-)$ complex with excess 9,10-dihydroanthracene (bond dissociation energy, $BDE_{C–H}$ = 78 kcal/mol) at −70 °C resulted in the formation of anthracene in good yield, with a 1:1 reaction stoichiometry. These results imply that the proposed $Fe^{III}$(OOH) intermediate reacts further with DHA radical, but this intermediate was not identified. A kinetic analysis gave $k_2$ = 0.005 $M^{-1}$ $s^{-1}$ and KIE = 7 for the oxidation of DHA, pointing to rate-limiting H-atom abstraction. These results showed that a nonheme $Fe^{III}(O_2^-)$ species is capable of abstracting a H-atom from a C– H bond even at the low temperature of −70 °C.

More recently in 2015, a mixed-ligand system containing the tridentate hydrotris(3,5-dimethylpyrazolyl)borate ($Tp^{Me2}$) and the bidentate imidazolyl-based borate ligands [B-($Im^{N\text{-}Me}$)$_2$MePh]$^-$ ($L^{Ph}$) led to the characterization of a mononuclear iron(III)–superoxide complex (Scheme 6).[79] The hs-$Fe^{II}$ complex [$Fe^{II}(Tp^{Me2})(L^{Ph})$] reacted with $O_2$ at −60 °C to form brown [$Fe^{III}(O_2^-)(Tp^{Me2})(L^{Ph})$] ($\lambda_{max}$ = 350 nm). Resonance Raman spectroscopy revealed a Fermi doublet band at 1168 $cm^{-1}$ that shifted to 1090 $cm^{-1}$ upon $^{18}O$ substitution, and a low-energy vibration at 592 $cm^{-1}$ which was also sensitive to isotope substitution.

These bands can be assigned to the $\nu_{O-O}$ and $\nu_{Fe-O}$ modes respectively, of a bound superoxide species. In this case, Mössbauer spectra were not reported, but $^1$H NMR spectroscopy showed a sharp, diamagnetic spectrum, pointing to a ls-$Fe^{3+}$ center ($S = 1/2$) antiferromagnetically coupled with the superoxide anion ($S = 1/2$). An X-ray crystal structure of an analogous Co ($O_2^-$) complex with the $Tp^{Me2}$ and $O^iPr$-substituted $L^{OiPr}$ ligands was obtained. The superoxide ligand in the $Co^{III}$ complex was bound in an $\eta^1$ fashion, and by analogy it was assumed that the iron complex exhibited the same binding mode.

The [$Fe^{III}(O_2^-)(Tp^{Me2})(L^{Ph})$] complex exhibited similar UV–vis and rR features compared to [$Fe^{III}(O_2^-)$(BDDP)], which also contained an $\eta^1$-bound $O_2^-$ ligand.[77,79] However, the former complex was characterized as hs-$Fe^{III}$, whereas the latter complex was ls-$Fe^{III}$. This difference in spin state was proposed to be an important factor in the difference in reactivity between these two complexes. The ls-[$Fe^{III}(O_2^-)$-($Tp^{Me2}$)($L^{Ph}$)] is not capable of abstracting a H-atom from even weak C–H bonds such as found in 1-benzyl-1,4-dihydronico-tinamide (BNAH, $BDE_{C-H}$ = 67.9 kcal/mol), in contrast to the [$Fe^{III}(O_2^-)$(BDDP)], which was able to cleave the C–H bond in DHA ($BDE_{C-H}$ = 78 kcal/mol). The low spin complex can only abstract H-atoms from weak X–H bonds (X = O, N; $BDE_{X-H}$ < 73 kcal/mol) such as phenyl hydrazine, and 2-hydroxy-2-azaadamantane (AZADOL). One advantage of this system was that H-atom abstraction from these X–H substrates allowed for the spectroscopic identification (UV–vis, rR, EPR) of the $Fe^{III}$–OOH product, which could not be detected in the BDDP complex.

### 4.2. Formation of $Fe^{IV}$(O) Complexes: Intermediacy of the (Hydro)peroxo Intermediate

A high-valent $Fe^{IV}$(O) species has been proposed to be the key intermediate responsible for substrate oxidation in the catalytic cycle of many nonheme iron enzymes. The first spectroscopically characterized $Fe^{IV}$(O) in a nonheme iron enzyme was seen in studies on the α-keto acid dependent taurine dioxygenase in 2003.[80,81] Subsequently, ferryl species were detected and characterized in prolyl-4-hydroxylase,[82] halogenases SyrB2[83] and CytC3,[84] and aromatic amino acid hydroxylases tyrosine hydroxylase[85] and phenylalanine hydroxylase.[86] A common similarity among them is that they exhibit high-spin ($S = 2$) ground states.

For bioinorganic model systems, the first terminal oxo–iron complex synthesized from $O_2$ was reported in 2000.[87] A tripodal urea-based ligand, tris[(*N*′-*tert*-butylureaylato)-*N*-ethyl)]aminato ($(H_3buea)^{3-}$), was used to stabilize this metal–oxo complex via intramolecular H-bonding interactions with the terminal oxo ligand. The oxidation state of the iron center in this case was +3, not +4, leading to the unusual stabilization of a lower-valent $Fe^{III}$(O) complex. The proposed mechanism (pathway A, Scheme 7) for the reaction involves a peroxo-bridged diiron(III) complex [1,2-μ-$O_2$-($Fe^{III}H_2buea)_2$]$^{2-}$. Subsequently, the peroxo bond undergoes O–O bond homolysis to form a putative $Fe^{IV}$(O) species. A H-atom abstraction reaction from an exogenous C–H bond followed by an intramolecular proton transfer yields the final $Fe^{III}$(O) complex. It was later shown that this $Fe^{III}$(O) species could be oxidized to an $Fe^{IV}$(O) complex by ferrocenium tetrafluoroborate at −60 °C.[88] X-ray crystallographic characterization of [$Fe^{IV}(O)(H_3buea)]^-$ revealed a short Fe–O distance

(1.680(1) Å), and parallel mode EPR spectroscopy (X-band, 10 K) revealed resonances at $g$ = 8.19, g = 4.06 indicative of a high-spin ($S$ = 2) manifold. This complex is one of the few examples of a synthetic hs-$Fe^{IV}$(O) complex, and the only one derived from $O_2$.[89–93]

The first spectroscopic observation of an $Fe^{IV}$(O) intermediate, obtained directly from the reaction of $O_2$ with an iron precursor complex, was reported in 2005.[94] The iron-cyclam derivative [$Fe^{II}$(TMC)$(OTf)_2$] (TMC = 1,4,8,11-tetramethyl-1,4,8,11-tetraazacyclotetradecane) was inert to $O_2$ in $CH_3CN$, but was made reactive with $O_2$ upon changing the solvent to a mixture of $CH_3CN$/solv (1:1) (solv = EtOH, $Bu_2O$, THF). The resulting pale green species exhibited a broad, relatively weak UV–vis feature at $\lambda_{max}$ = 825 nm ($\varepsilon$ = 370 $M^{-1}$ $cm^{-1}$), which was similar to that previously reported for [$Fe^{IV}$(O)(TMC)$(CH_3CN)]^{2+}$ (prepared from PhIO as the oxidant).[95] These data suggested the formation of the $Fe^{IV}$(O) species under the mixed-solvent conditions. The marked difference in reactivity for the [$Fe^{II}$(TMC)$(OTf)_2$] complex with $O_2$ in different solvents was attributed to the influence of the solvent on the $Fe^{III}/Fe^{II}$ redox potential. The $E_{1/2}$ value for the $Fe^{III}/Fe^{II}$ couple in a mixed $CH_3CN$/solv (1:1) combination is more positive when solv = $CH_3CN$ (0.01 V), acetone (0.08 V), and $CH_2Cl_2$ (0.02 V), as compared to a more negative potential when solv = butyl ether (−0.28 V) or THF (−0.14 V). The latter two solvent combinations allowed for the activation of $O_2$ by the $Fe^{II}$ complex, providing strong evidence that the solvent-tuned $Fe^{III}/Fe^{II}$ redox potential was a critical factor in promoting $O_2$ activation. A plausible mechanism for the generation of [$Fe^{IV}$(O)(TMC)$(CH_3CN)]^{2+}$ is through a diiron peroxo-bridged intermediate (pathway B, Scheme 7), although no evidence for this mechanism was presented. In a later study, it was argued that the binding of alcohol or ether to the proposed μ-1,2-peroxodiiron(III) intermediate may facilitate the homolysis of the O–O bond, providing a rationale for the formation of $Fe^{IV}$(O) in the mixed solvent system.[96] A similar observation was made for iron–porphyrin, where amines were proposed to coordinate in the axial position of the metal and facilitate O–O cleavage in a peroxide-bridged intermediate.[28–29] The formation of a dimeric peroxo-bridged structure from the reaction of monomeric $Fe^{II}$ complex + $O_2$ was demonstrated in a separate study utilizing hydrotris-(pyrazol-1-yl)borate-bound iron(II)–diketonate complex.[97]

The influence of an additional, covalently linked axial donor atom on the $O_2$ reactivity of the $Fe^{II}$(TMC) complex was examined by replacing one of the methyl groups in the TMC ligand with a 2-pyridylmethyl arm, giving the pentadentate ligand TMC-py (1-(2'-pyridylmethyl)-4,8,11-trimethyl-1,4,8,11-tetraazacyclotetradecane).[96] As seen for the parent six-coordinate [$Fe^{II}$(TMC)$(OTf)_2$] complex, the new five-coordinate [$Fe^{II}$(TMC-py)$]^{2+}$ complex was air-stable in $CH_3CN$. However, addition of stoichiometric amounts of a $BPh_4^-$ salt and the strong proton donor $HClO_4$ resulted in the rapid formation of [$Fe^{IV}$(O)(TMC-py)$]^{2+}$ ($\lambda_{max}$ = 834 nm, $\varepsilon$ = 260 $M^{-1}$ $cm^{-1}$) (pathway D, Scheme 7). The identification of phenol (PhOH) and biphenyl byproducts indicated that $BPh_4$-was serving as a reductant during the $O_2$ reaction according to the following reaction: $BPh_4^- - e^- \rightarrow BPh_4^{\bullet} \rightarrow BPh_3 + Ph^{\bullet}$. The requirement of a 1:1:1 ratio of $Fe^{II}/H^+/BPh_4^-$ for the maximal formation of $Fe^{IV}$(O) suggested the intermediacy of an iron(III)–hydroperoxo ($Fe^{III}$–OOH) complex in which one electron from $Fe^{II}$ and one electron from $BPh_4^-$ reduce $O_2$ to the peroxide level. However, the peroxide intermediate could not be trapped for spectroscopic characterization.

In 2009, a similar approach of using external $H^+$ ($HClO_4$) and $e^-$ (BNAH) sources was successfully employed to trap an $Fe^{III}$–OOH species during $O_2$ activation by $[Fe^{II}(N4Py)]^{2+}$ (N4Py = *N*,*N*-bis(2-pyridylmethyl)-*N*-bis(2-pyridyl)-methylamine) and $[Fe^{II}(Bn\text{-}TPEN)]^{2+}$ (Bn-TPEN = *N*-benzyl-*N*,*N*′,*N*′-tris(2-pyridylmethyl)-1,2-diaminoethane) complexes (pathway E, Scheme 7).[98] In these cases, the dioxygen reactivity was achieved in $CH_3OH$, instead of the previously used aprotic $CH_3CN$. Both the N4Py and Bn-TPEN complexes exhibited ls-$Fe^{II}$ ($S = 0$) centers in $CH_3CN$, but gave hs-$Fe^{II}$ complexes with $CH_3OH$ as solvent. The change in spin state was accompanied by a change in $Fe^{III}/Fe^{II}$ redox potentials. The hs-$Fe^{II}$ complexes exhibited significantly lower redox potentials than their low-spin counterparts. As the lower $Fe^{III}/Fe^{II}$ redox potentials favors oxidation of $Fe^{II}$, hs-$Fe^{II}$ complexes are well-suited to activate $O_2$. These results demonstrate the importance of solvent effects on the spin state of an iron complex, which in turn, can influence the $O_2$ reactivity of such complexes.[98]

When the $[Fe^{II}(TMC)(OTf)_2]$ complex was exposed to similar $H^+/e^-$ sources with the addition of $HClO_4$ ($H^+$) and BNAH ($e^-$) in pure $CH_3CN$, the activation of $O_2$ was facilitated, but proceeded directly to the $Fe^{IV}(O)$ complex without the observation of an $Fe^{III}(OOH)$ intermediate (pathway D, Scheme 7).[98] The instability of the $Fe^{III}(OOH)$ intermediate in this case was suggested as the likely reason for the inability to trap this species. The same strategy of combining external $H^+/e^-$ ($HClO_4/BPh_4^-$) sources with $O_2$ was employed in 2010 to give another example of an $Fe^{III}OOH$ complex generated from a hs-$Fe^{II}$ complex (pathway E, Scheme 7).[99] A TPEN-based ligand ($L_5{}^2aH$) was used in this work that incorporated a H-bond donor (pivalamido substituent) to stabilize and trap the $Fe^{III}OOH$ complex.

The Brönsted acids ($H^+$) used in the former $Fe^{II}$-mediated $O_2$ activation processes can be replaced with Lewis acids (LAs) such as $Sc(OTf)_3$. In 2013, The $O_2$-derived formation of $[Fe^{IV}(O)(TMC)(CH_3CN)]^{2+}$ using $NaBPh_4$ and $Sc(OTf)_3$ in $CH_3CN$ was described.[100] It was proposed that the $Sc^{3+}$ binds to a putative iron(III)–peroxo intermediate to form a $Fe^{3+}$–($\mu$–$\eta^2$:$\eta^2$–$O_2$)-$Sc^{3+}$ core, which promotes O–O bond cleavage and formation of the $Fe^{IV}(O)$ species. The plausibility of a species like $Fe^{3+}$–($\mu$–$\eta^2$:$\eta^2$-$O_2$)–$Sc^{3+}$ was independently demonstrated by preparing this species from the reaction of $Fe^{III}OOH$ with $Sc(OTf)_3$. However, a later report has suggested that this reaction occurs via a more complex $Sc^{3+}$-promoted autocatalytic radical chain pathway, rather than via direct $O_2$ activation.[101] The addition of Brönsted and Lewis acids to facilitate the $O_2$ activation process is reminiscent of the “push–pull” mechanism, well-developed for heme enzymes such as the peroxidases.[4] In the biological systems, protons are carefully shuttled to an iron-bound dioxygen species by nearby protein residues to facilitate cleavage of the O–O bond and release of the distal O-atom as water. In the synthetic systems, simple bimolecular interactions with appropriate $H^+$ or LA metal ions in sufficient concentrations appear to have a similar effect, although the structural aspects and exact timing of formation of the M–OO–$H^+$ (or LA) intermediates are generally not well understood. These interactions are worthy of future study, as are the development of porphyrinoid ligands with tethered groups for shuttling protons or creating hydrogen bonds with $M/O_2$-derived intermediates.

Most of the examples described above relied on the use of external proton and electron sources to reduce $O_2$ and generate $Fe^{III}OOH$ or $Fe^{IV}(O)$ complexes.[96,98,99] These separate proton and electron sources can also be replaced with a single H-atom donor to form a nonheme $Fe^{IV}(O)$ complex (pathway C, Scheme 7).[102] It was noted before that the $[Fe^{II}(TMC)\text{-}(OTf)_2]^{2+}$ is air-stable in $CH_3CN$. However, the $Fe^{II}$–TMC complex in the presence of an olefin such as cyclohexene, cycloheptene, or cyclooctene led to the rapid formation of an $Fe^{IV}(O)$ complex in high yield (>90%). A linear correlation between the rate of $Fe^{IV}(O)$ formation and the allylic C–H bond strengths of the alkenes, along with a large KIE, indicated that C–H bond breaking was the rate-determining step. It was proposed that a putative $Fe^{III}(O_2^{-})$ complex abstracts an H-atom from the olefinic substrate to form the $Fe^{III}OOH$ intermediate and alkenyl radical. The alkenyl radical could undergo a rebound reaction with $Fe^{III}OOH$ to give the $Fe^{IV}(O)$ species. Recently in 2015, formation of iron(III)–peroxo and iron (IV)–oxo complexes were shown with the same ligand platform TPEN.[103] However, reductive activation of dioxygen in this case was achieved electrochemically.

More recently in 2016, an unusual example of the two-electron reduction of $O_2$ at a single iron center to form an iron–peroxo intermediate was described for an organometallic precursor.[104] In this case both of the reducing equivalents were provided by the $Fe^{II}$ center, leading to an iron(IV)–peroxo complex. The X-ray crystallographic structures of the heterodinuclear $[Ni^{II}Fe^{II}]$ complexes $[Ni^{II}LFe^{II}(RCN)(\eta^5\text{-}C_5Me_5)]^+$ (L = *N,N′*-diethyl-3,7-diazanonane-1,9-dithiolato, R = Et, Me) (Scheme 8) revealed that the $Ni^{II}$ and $Fe^{II}$ ions are bridged by two thiolato units of the ligand L. The spin state of the $Fe^{II}$ ion was characterized as low-spin ($S = 0$) by various spectroscopic techniques, including Mössbauer, ESR, and $^1H$ NMR spectroscopy. This complex is one of the few examples of a ls-$Fe^{II}$ complex that is capable of $O_2$ activation. The strong electron-donating nature of the $\eta^5\text{-}C_5Me_5$ (Cp*) ligand may facilitate $O_2$ reduction at ls-$Fe^{II}$ in this system.[104]

Both the $Fe^{II}(CH_3CN)$ and $Fe^{II}(EtCN)$ complexes reacted with $O_2$ at low temperature (−40 and −80 °C for MeCN and EtCN, respectively) to form a brown species with charge-transfer bands at 410 nm ($\varepsilon$ = 3000 $m^{-1}$ $cm^{-1}$) and 520 nm ($\varepsilon$ = 1500 $m^{-1}$ $cm^{-1}$), which was crystallized in $CH_3CN/Et_2O$. The crystal structure (Scheme 8) revealed that the $O_2$ molecule was coordinated to the Fe center in an $\eta^2$ (side-on) manner. The O–O bond distance (1.381(3) Å) was consistent with the $O_2$ being reduced to the peroxide level, as seen in other side-on metal–peroxo complexes.[105–108] However, this distance is slightly shorter than the O–O distance found in another crystallographically characterized complex, $[Fe^{III}(TMC)\text{-}(OO)]^+$ (O–O = 1.463(6) Å).[109] Isotope labeling experiments with $^{18}O_2$ confirmed $O_2$ as the sole source of oxygen in the complex, although addition of $H_2O_2$ also led to facile exchange of the side-on-bound peroxide ligand. Mössbauer parameters ($\delta$ = 0.42 mm $s^{-1}$, $\Delta E_Q$ = 0.33 mm $s^{-1}$) supported the assignment of a +4 oxidation state for the Fe center, and variable-temperature magnetic susceptibility measurements revealed a low-spin ($S = 0$) diamagnetic ground state for the complex. The high-valent $Fe^{IV}$ complexes, obtained in synthetic biomimetic systems, are normally intermediate-spin $S = 1$ complexes.[110] Thus, this peroxo complex is a rare example of a ls-$Fe^{IV}$ ($S = 0$), likely due to the strong-field Cp* donor. Addition of the $e^-$source $BH_4^-$ in combination with the $H^+$ donor EtOH to $[Ni^{II}LFe^{IV}(\eta^2\text{-}O_2)(\eta^5\text{-}C_5Me_5)]^+$ at −40 °C led to the reduction of peroxide to $H_2O$. A very modest TON =

1.3 was achieved. This work provided an example where $4e^-$ reduction of $O_2$ was carried out at a nonheme iron center and both oxygen atoms in $O_2$ were reduced to $H_2O$.

### 4.3. Nonheme Iron-Mediated Substrate Oxidations Utilizing Dioxygen

There are a number of reports over the years where $O_2$ has been used by nonheme iron complexes to oxidize organic substrates. Herein we focus on some of the select examples of these systems in recent years and categorize them in different subclasses based on the type of substrates that gets oxidized.

**4.3.1. Aromatic C–C Bond-Cleaving Reactions—**Cleavage of the C–C bonds, particularly in aromatic substrates, is an important class of reactions performed by a number of nonheme iron enzymes, including the intra- and extradiol-cleaving catechol dioxygenases and 2-aminophenol dioxygenase. These enzymes play a crucial role in the biodegradation of the aromatic compounds in bacterial systems. Diol-cleaving dioxygenases utilize a mononuclear iron center and convert catechol substrates to ring-opened products, whereas aminophenol dioxygenase acts on 2-aminophenol substrate to form the ring-opened 2-aminomuconic acid semialdehyde, which then loses water to form an aromatic ring (Scheme 9).[111,112]

A number of synthetic model complexes have been prepared that exhibit intra- and extradiol cleavage activity, and a comprehensive review published in 2004 provided an account of these complexes.[6] Extradiol/intradiol dioxygenase activity by nonheme iron complexes was shown with bis(1-alkylimidazol-2-yl)propionate ($L^-$) ligands (Scheme 10).[111] Each ligand provides two imidazolyl N-atoms and a carboxylate O-atom for metal coordination, mimicking the 2-his-1-carboxylate binding motif observed in the extradiol cleaving dioxygenase. The [$Fe^{II}$(L)(Hdtbc)] complexes (Hdtbc = monodeprotonated 3,5-di-*tert*-butylcatechol), prepared *in situ*, reacted rapidly with $O_2$ to give respective [$Fe^{III}$(L)(dtbc)] complexes. The UV–vis spectrum for the reaction mixture after $O_2$ reactivity (324, 490, 800 nm) matched well with that of independently synthesized [$Fe^{III}$(L)(dtbc)] complexes. The initially formed [$Fe^{III}$(L)-(dtbc)] underwent a subsequent slow $O_2$ reaction to give oxidized organic product(s) (Scheme 10). The nature of the product(s) after the completion of the reaction was dependent on the solvent. Performing the reaction in $CH_3CN$ led to exclusive formation of the auto-oxidation product 3,5-di-*tert*-butylbenzoquinone, whereas both the auto-oxidation product (major) and intradiol cleavage products (minor) were obtained in $CH_3OH$. Interestingly, non-coordinating solvents such as $CH_2Cl_2$ led to almost equimolar formation of both the intra-and extradiol cleavage products. This result was consistent with the hypothesis that extradiol cleavage product formation is favored when the metal center has a vacant site for dioxygen binding.[111,113,114] Although the complexes were not selective for either type of cleavage pathway, addition of the proton donor, $[Et_3NH]BF_4$ increased the selectivity toward extradiol cleavage products. In a similar study, the carboxylate arm of the ligand L was replaced with a phenolate unit to mimic the active site coordination environment of intradiol cleaving dioxygenase.[115] However, no greater selectivity for intra- or extradiol cleavage pathway was observed when the $Fe^{III}$ complex of the new ligand was reacted with $O_2$.

In 2008, dioxygenase reactivity of a number of $Fe^{III}$-catecholate complexes with tetradenatate N4 ligands were investigated (Figure 3a).[116] The oxygenation reaction of the $Fe^{III}$ complexes $[L'Fe^{III}(Hdtbc)]^{2+}$ with a monodeprotonated 3,5-di-*tert*-butylcatechol unit gave predominantly extradiol cleavage products. The fully deprotonated complex $[L'Fe^{III}(dtbc)]^{+}$ led to a higher yield for the intradiol cleavage products. It was proposed that an internal proton transfer from the −OH group to one of the *cis*-pyridyl rings in the monodeprotonated complex resulted in a vacant coordination site (as the protonated pyridine is a very weak donor) at the $Fe^{III}$ center for $O_2$ binding (Figure 3a). As mentioned before, the availability of the vacant $O_2$ binding site was postulated to be a critical component for the extradiol cleavage pathway.

A higher selectivity for intradiol cleavage products was obtained when a series of five-coordinate $Fe^{III}$ complexes with isoindoline-based ligands were reacted with $O_2$ (Figure 3b).[117] Fully deprotonated 3,5-di-*tert*-butyl catechol was employed as the substrate and was shown to coordinate with the iron center in a bidentate manner. Here the meridional geometry imposed by the $N_3$ donors of isoindoline was proposed to play a crucial role toward the observed intradiol selectivity for the reaction.[117]

The C–C bond cleavage reactivity of synthetic nonheme iron complexes was studied for a 2-aminophenol substrate as well.[112,118–121] Dioxygen reactivity was studied for the nonheme $Fe^{II}$ complex $[(6\text{-}Me_3\text{-}TPA)Fe^{II}(4\text{-}tBu\text{-}HAP)]\text{-}(ClO_4)$, which was prepared using tetradentate 6-$Me_3$-TPA (6-$Me_3$-TPA = tris(6-methyl-2-pyridylmethyl)amine) and bidentate 4-tBu-HAP (4-tBu-HAP = monoanionic 2-amino-4-*tert*-butylphenolate) ligand (Figure 3c).[119] Reaction of $[(6\text{-}Me_3\text{-}TPA)Fe^{II}(4\text{-}tBu\text{-}HAP)](ClO_4)$ with $O_2$ in $CH_3CN$ immediately formed a metastable $Fe^{III}$ complex (UV–vis and EPR spectra matched well with the independently prepared $Fe^{III}$ complex) with absorption bands at 366, 600, and 934 nm. The $1e^-$-oxidized $Fe^{III}$ complex, formed immediately after the reaction of $Fe^{II} + O_2$, slowly converted into the $[(6\text{-}Me_3\text{-}TPA)Fe^{III}(4\text{-}tert\text{-butyl-2-picolinate})]^{+}$ complex ($\lambda_{max}$ = 660 nm), which was supported by EPR and ESI-MS experiments. $^1H$ NMR and GC-MS analysis of the organic products also revealed the formation of 4-*tert*-butyl-2-picolinate, an extradiol cleavage product for 4-tBu-HAP. This is in contrast with the dioxygen reactivity of an analogous $[(6\text{-}Me_3\text{-}TPA)Fe^{II}(dtbc)]^{+}$ (dtbc =3,5-di-*tert*-butylcatecholate) and other $Fe^{II}$–catecholate complexes with tetradentate ligands, where C–C bond cleavage was observed to follow an intradiol pathway.[6,116]

**4.3.2. Synthetic Models for α-Keto/Hydroxy Acid-Dependent Enzymes—**α-Keto gluatarate-dependent enzymes are the largest subclass of nonheme iron enzymes that perform a wide range of organic transformations, including hydroxylation, desaturation, and ring closure.[122] As the name suggests, α-keto glutarate cofactor is required for enzyme activity, and the binding of this cosubstrate promotes dioxygen activation by the iron center. The α-keto glutarate undergoes a decarboxylation reaction to give succinate, incorporating one O-atom from $O_2$. A high-valent $Fe^{IV}(O)$ intermediate was proposed to be the key intermediate in these enzymes and was spectroscopically characterized in a number of cases.[80–84,123]

Despite being the largest member of the nonheme iron enzyme family, examples of synthetic functional model complexes of these systems that utilize $O_2$ are limited.[124,125] In 1999, dioxygen reactivity of an $Fe^{II}$ complex, coordinated with hydrotris(3,5-diphenylpyrazol-1-yl)borate ($Tp^{Ph2}$) and benzoylformate (BF), was reported.[125,126] The iron(II) complex [$Fe^{II}(Tp^{Ph2})$(BF)] was shown to react with $O_2$ at room temperature to form an arene hydroxylated [$Fe^{III}(Tp^{Ph2*})$(OBz)] complex (Scheme 11). Although an $Fe^{IV}$(O) species was postulated to be the active oxidant, it was not detected by spectroscopic methods. In a subsequent study, it was shown that the $Fe^{IV}$(O) complex could be intercepted in the presence of external substrates such as thioanisole and cyclohexene (Scheme 11).[127] When the oxygenation reaction of [$Fe^{II}(Tp^{Ph2})$(BF)] was performed in the presence of thioanisole, no ligand hydroxylation reaction was observed. Instead, decarboxylation of benzoylformate (BF) to benzoate (OBz) was observed along with the formation of methyl phenyl sulfoxide (70%). The C–H bond substrates such as DHA and cyclohexene were also used to intercept the putative $Fe^{IV}$(O) species in the oxygenation reaction.

Dioxygen reactivity of $Fe^{II}$-α-hydroxy acid complexes received some attention lately[128–132] and were prepared as functional models for the enzyme CloR.[133] The synthetic $Fe^{II}$ complex [$Fe^{II}(Tp^{Ph2})$(benzilate)] reacted with $O_2$ in benzene to form an $Fe^{III}$-phenolate complex ($\lambda_{max}$ = 600 nm), along with the quantitative formation of benzophenone (generated from the decarboxylation of benzilate) (Scheme 12).[132] The proposed mechanism for this reaction involves initial formation of an $Fe^{III}(O_2^{-})$ species that abstracts a H-atom from the hydroxyl group to generate an $Fe^{III}$OOH complex. A subsequent O–O bond cleavage reaction would form an $Fe^{IV}$(O)–OH complex, which was proposed to be the active oxidant for the ligand hydroxylation reaction. Although none of the proposed intermediates were characterized spectroscopically, the $Fe^{IV}$(O) oxidant was intercepted with a number of external substrates such as fluorene, cyclohexene and thioanisole.[131] A subsequent study on the interception reactions with sulfides and cyclohexene revealed a nucleophilic reactivity profile for the oxidant, which was confirmed by a Hammett analysis (Scheme 12).[130] The possibility of an $Fe^{II}$OOH or an $Fe^{IV}$(O)–OH species was implicated in the absence of direct spectroscopic evidence.

Interestingly, the presence of a LA (for example $Sc(OTf)_3$) in the reaction of [$Fe^{II}(Tp^{Ph2})$(benzilate)] with $O_2$ switched the nature of the oxidant from being nucleophilic to electrophilic (Scheme 12).[129] Interception of the active oxidant with thioanisole substrate gave sulfoxide product only, whereas both the sulfoxide and sulfone were obtained previously in absence of $Sc(OTf)_3$. Hammett analysis with *para*-substituted ArSMe substrates revealed a negative ρ value (−0.929), which was suggestive of an electrophilic oxidant. A negative ρ value was obtained for various *para*-substituted styrene substrates as well. An electrophilic $Fe^{IV}$(O)–OH species was implicated as the active oxidant here. The LA was proposed to facilitate the heterolytic cleavage of the O–O bond in the intermediate $Fe^{II}$(OOH) species, leading to the formation of the $Fe^{IV}$(O)– OH complex. It was shown that a protic acid (for e.g. pyridinium perchlorate) could also be used, instead of a LA, to generate the electrophilic oxidant.[128] Interestingly, addition of a chloride source into the reaction made the oxidant much more electrophilic (based on Hammett analysis) and led to C–H halogenation along with C–H hydroxylation (Scheme 12). The intermediacy of an

iron(IV)–oxo–chloride complex was hypothesized to explain the observed hydroxylation/halogenation reactivity.[128]

**4.3.3. S-Oxygenation Reactions: Dioxygen Reactivity of Iron–Thiolate Complexes—**Dioxygen activation by thiolate-ligated iron complexes is of particular biological relevance because of a range of nonheme iron enzymes that activate $O_2$ and employ one or more cysteinate ligands. One example is cysteine dioxygenase (CDO), a nonheme iron enzyme that carries out the dioxygenation of cysteine to cysteine sulfinic acid. The CDO enzyme contains a mononuclear iron active site with three histidine ligands in a facial triad, which is different from the usual two histidine-1-carboxylate binding motif found in most of the other mononuclear nonheme iron enzymes. This enzyme is part of a larger group of related enzymes that can be classified as thiol dioxygenases (cysteamine dioxygenase, cysteine dioxygenase, 3-mercaptopropionate dioxygenase).[134] These enzymes are related in that they utilize $O_2$ to convert sulfur substrates to the dioxygenated sulfinic acid products. A number of mechanisms were proposed which involves formation of various iron–oxygen intermediates prior to the *S*-oxygenation reaction.[135–139] However, there is currently no direct experimental evidence for any of these $O_2$-derived intermediates. Simplified synthetic model complexes can sometimes provide better access to the trapping and characterization of analogous Fe/$O_2$ intermediates, with greater flexibility in tuning electronic and steric properties. In recent years, efforts have been undertaken to study the dioxygen reactivity of various mononuclear, thiolate-ligated iron(II) compounds with biomimetic ligand environments.

Controlling the oxygenation of sulfur coordinated to iron(II) is challenging because of the potentially facile oxidation of both Fe and S centers, and the possible range of products that could form. Until 2010, previous reports on $Fe^{II}(SAr) + O_2$ chemistry described the formation of oxo-bridged dinuclear iron complexes or disulfide products.[134] An *S*-oxygenation reaction (Scheme 13) occurring from $Fe^{II}(SAr) + O_2$ was described by our group in 2010.[140] A bis-imino pyridine (BIP) ligand (described as $LN_3S$) providing three neutral N donors and a tethered thiolate donor was used in the former study. Reaction of $[Fe^{II}(LN_3S)(OTf)]$ with $O_2$ in $CH_2Cl_2$ (or in MeCN, THF) resulted in an immediate color change, and MS analysis of the reaction mixture was consistent with sulfonate formation (i.e., triple oxygenation at S). Quantitative reversed-phase HPLC confirmed production of the triply *S*-oxygenated ligand. Isotope labeling ($^{18}O_2$, $H_2{}^{18}O$) proved that oxygen gas was the sole source of O-atoms in the sulfonato complex. The lack of an EPR signal for the final product indicated that the oxygenated complex was in the $Fe^{II}$ state. The necessity of a redox-active Fe center to mediate *S*-oxygenation was demonstrated by the synthesis of the Zn-analogue $[Zn^{II}(LN_3S)(OTf)]$, which showed no reactivity toward $O_2$. This work presented the first selective *S*-oxygenation reaction derived from the reaction of $Fe^{II}SAr + O_2$.

Subsequently in 2011, we described the dioxygen reactivity of two new bis-imino pyridine-based $Fe^{II}SAr$ complexes, $[(^{iPr}BIP)\text{-}Fe^{II}(SPh)(Cl)]$ and $[(^{iPr}BIP)Fe^{II}(SPh)(OTf)]$ [$^{iPr}BIP$ = 2,6-$(ArN{=}CMe)_2C_5H_3N$, Ar = 2,6-$^{i}Pr_2C_6H_3$] (Scheme 13).[141] However, unlike the previous example of $[Fe^{II}(LN_3S)(OTf)]$, the thiolate ligand was added from an exogenous source and not tethered to the BIP ligand. The complexes were prepared from the reaction of

[($^{iPr}$BIP)$Fe^{II}(X)_2$] (X = Cl, OTf) with NaSPh. The presence of hs-$Fe^{II}$($S$ = 2) in both complexes was confirmed by X-ray crystallography and $^1$H NMR spectroscopy (in $CD_2Cl_2$).

The binding of the exogenous thiolate ligand to [($^{iPr}$BIP)-$Fe^{II}(X)^2$] facilitated dioxygen activation by the resulting $Fe^{II}$SAr complexes. The [($^{iPr}$BIP)$Fe^{II}$(SPh)(Cl)] complex with a $PhS^-$ligand in a pseudoaxial position reacted with excess $O_2$ in $CH_2Cl_2$ to form a green species ($\lambda_{max}$ = 690 nm, $\varepsilon \approx 1500\ M^{-1}\ cm^{-1}$) (Scheme 13). The UV–vis features, mass-spectrometric data and the labeling experiments with $^{18}O_2$ were suggestive of an iron–oxo product. The sulfur component was oxidized to disulfide (PhS-SPh) (85% yield). In comparison, the complex [($^{iPr}$BIP)$Fe^{II}$(SPh)(OTf)] which has the thiolate group in the pseudoequatorial position, reacted with $O_2$ to form an $S$-oxygenated $Fe^{II}(SO_3Ar)$ complex (Scheme 13). The ability of both the [($^{iPr}$BIP)$Fe^{II}$(SPh)(Cl)] ($E_{1/2}$ = −0.173 V vs $Fc^+$/Fc) and [($^{iPr}$BIP)$Fe^{II}$(SPh)(OTf)] ($E_{1/2}$ = −0.372 V) to activate $O_2$ was attributed in part to their relatively low $Fe^{III}/Fe^{II}$ redox potentials. The nonthiolate-ligated [($^{iPr}$BIP)$Fe^{II}(Cl)_2$] ($E_{1/2}$ = 0.025 V) and [($^{iPr}$BIP)$Fe^{II}(OTf)_2$] ($E_{1/2}$ = 0.613 V) have significantly more positive $E_{1/2}$ values, and do not show any reactivity toward $O_2$. The difference in reactivity for [($^{iPr}$BIP)-$Fe^{II}$(SPh)(Cl)] versus [($^{iPr}$BIP)$Fe^{II}$(SPh)(OTf)] can be attributed to structural features. The former complex has a potential $O_2$ binding site *trans* to the SPh group, whereas the latter complex has an open site *cis* to the SPh ligand. The *cis* orientation for [($^{iPr}$BIP)$Fe^{II}$(SPh)(OTf)] allows for close approach of a putative iron-bound superoxide toward the sulfur donor, leading to intramolecular $S$-oxygenation. This same process is not favored for the *trans* position of the $O_2$ binding site, and thus [($^{iPr}$BIP)$Fe^{II}$(SPh)(Cl)] does not undergo $S$-oxygenation, but instead only gives disulfide.

These initial CDO model complexes led to triply oxygenated sulfur products.[140,141] Our first evidence for the formation of an iron(II)–sulfinate complex from $Fe^{II}$–SR/$O_2$ was obtained with a new tetradentate ligand, N3PySH, which allows for facial N3 coordination to the iron center and a *cis* orientation of the thiolate donor to the open site on the metal, as seen in the CDO active site.[142] The resulting [$Fe^{II}$(N3PyS)($CH_3CN$)]-($BF_4$) complex reacted with $O_2$ in $CH_3OH$ to form a doubly oxygenated sulfinate complex which was crystallized in the presence of $SCN^-$ to give the neutral product [$Fe^{II}$(N3P$ySO_2$)-(SCN)] (Scheme 14). The crystal structure revealed that the sulfinate group was bound through the S-atom to the iron center. The IR spectrum of the sulfinate complex revealed peaks at 1129 and 1012 $cm^{-1}$, which were assigned to the asymmetric and symmetric S–O stretching modes, respectively.

Another example of a CDO model complex was reported at about the same time and described a thiolate-ligated tris-(pyrazolyl)borate complex [$Tp^{Me,Ph}$ $Fe^{II}$(CysOEt)], in which the sulfur donor comes from cysteine ethyl ester (Scheme 14).[143] This complex reacted slowly (5–6 h) with $O_2$ in $CH_2Cl_2$, and ESI-MS together with isotope labeling ($^{18}O_2$) experiments suggested formation of a doubly oxygenated complex. Mixed labeling experiments with $^{16}O_2$ /$^{18}O_2$ (1:1) indicated that both O-atoms in the product came from the same $O_2$ molecule. Although crystallographic evidence for the dioxygenated complex was lacking, evidence for sulfinate formation came from isolation of the organic product. In a subsequent report, a similar $S$-oxygenation reaction was observed with the related cysteamine complex [$Tp^{Me,Ph}Fe^{II}$-($SCH_2CH_2NH_2$)].[144] It should be mentioned that there is also related work on a well-defined chromium(III)–superoxo complex, derived from $Cr^{II}$ and

$O_2$, that reacts with thioether substrates to give sulfoxide products. This system was discussed in the context of the proposed mechanism for CDO.[145]

## 5. NONHEME MANGANESE COMPLEXES AND DIOXYGEN

Nonheme manganese centers play important roles in a number of metalloenzymes, such as superoxide dismutase, the oxygen-evolving complex in photosystem II, and ribonucleotide reductase.[9,10] In synthetic chemistry, Mn has been targeted for catalyzing the oxidation of organic substrates (e.g., epoxidation), as well as inorganic substrates such as water for renewable energy applications. Studies on the dioxygen reactivity of nonheme Mn complexes goes back to the 1970s. One of the first examples of the reaction of a $Mn^{II}$ complex with $O_2$ was reported in 1978, in which a peroxo-bridged dimeric $Mn^{III}$ complex was proposed.[146,147] However, subsequent studies with similar $Mn^{II}$ complexes indicated that the product was more likely an oxo-bridged $Mn_2^{III}$ complex.[148] In fact, most of the early reports on the activation of $O_2$ by Mn complexes describe the formation of oxo-bridged multinuclear structures.[148–152] A few studies reported the formation of mixed oxo/peroxo-bridged complexes.[150,151] However, the reaction mechanism and relevant "Mn–$O_2$" intermediates were not defined in most cases. The past few years has seen some development in mononuclear nonheme Mn chemistry, including the characterization of "Mn–$O_2$" species. These studies have led to new mechanistic information, including the identification of different factors that contribute to the reactivity of Mn with $O_2$.

Dioxygen-derived Mn–superoxo species are extremely rare for the nonheme systems. A stable $Mn^{III}(O_2^{-})$ species was generated in 2011 using a calixarene ligand platform and was structurally characterized by XRD.[153] The peroxo complexes were characterized for a number of nonheme Mn systems. An example of a mononuclear $Mn^{III}$–peroxo complex, which was synthesized from the reaction of a $Mn^{II}$ complex and dioxygen, was reported in 2008.[154] A derivative of the tren ligand, $H_2$bupa, which contains two substituted urea arms and one carboxyamidopyridyl donor, was employed in this study. The ligand substituents provide H-bonding groups that can help stabilize a peroxo-bound complex. The five-coordinate $Mn^{II}$ complex $[Mn^{II}H_2bupa]^{-}$ reacted with $O_2$ in the presence of diphenyl hydrazine (DPH) at room temperature to form a green $Mn^{III}$–peroxo complex with UV–vis maxima at $\lambda_{max}$ = 660 nm, 490 nm(sh) (Scheme 15). Characterization by FTIR and ESI-MS along with isotope labeling ($^{18}O_2$) studies supported the formation of a monomeric $Mn^{III}$–peroxo species, $[Mn^{III}H_3bupa(O_2)]^{-}$. Parallel mode EPR spectroscopy revealed a spectrum consistent with a quintet ($S$ = 2) Mn ion, which was quantified as 80% of the sample and indicated a +3 oxidation state. However, the protonation state of the peroxo ligand could not be conclusively determined, with either an $\eta^1$-hydroperoxo or an $\eta^2$-peroxo species as possibilities (Scheme 15). It was proposed that a $Mn^{III}$–superoxo intermediate forms initially and then abstracts a H-atom from DPH to give a $Mn^{III}$–hydroperoxo complex. The expected DPH product, azobenzene, forms nearly quantitatively in this reaction. The $Mn^{III}(OOH)$ complex can convert to an $\eta^2$-peroxo species by intramolecular proton transfer from $Mn^{III}(OOH)$ to the deprotonated carboxamido arm.

The peroxo complex $[Mn^{III}H_3bupa(O_2)]^{-}$ slowly converted into a $Mn^{III}O(H)$ species, which was characterized by UV–vis ($\lambda_{max}$ = 677 nm), ESI-MS, Evan's method, and X-ray

crystallography.[155] The hydroxyl proton was shared between the oxo ligand and a N-atom of the carboxamido unit. Interestingly, addition of the H-atom donor DPH to $[Mn^{III}O\text{-}(H)(H_2bupa)]^-$ led to production of $H_2O$ and regeneration of the $Mn^{II}$ complex (Scheme 15). Thus, the $[Mn^{II}H_2bupa]^-$ complex can serve as a catalyst for the reduction of $O_2$ to $H_2O$, and performing the oxygenation reaction of $[Mn^{II}H_3bupa]^-$ in the presence of excess DPH (20 equiv) produced azobenzene and $H_2O$ in excellent yields.

The first example of a structurally characterized $Mn^{III}$– peroxo complex derived from $Mn^{II}$ + $O_2$ was not reported until 2013.[13,156] A pentadentate ligand, $HS^{Me2}N_4$(6-Me-DPEN), containing a –SH group was utilized to prepare the monomeric complex $[Mn^{II}(S^{Me2}N_4(6\text{-}Me\text{-}DPEN))](BF_4)$ (Scheme 16). The thiolate ligation to the Mn center promoted $O_2$ activation, and the 6-methyl substituents on the pyridine rings provided steric shielding to stabilize the peroxo intermediate. The peroxo species $\{[Mn^{III}(S^{Me2}N_4(6\text{-}Me\text{-}DPEN))]_2(\mu\text{-}O_2)\}^{2+}$ was generated with $O_2$ at −40 °C in MeCN ($\lambda_{max}$ = 640 nm). This species had a short lifetime even at −40 °C and converted to a dinuclear $Mn^{III}$ oxo-bridged structure within minutes. Resonance Raman spectroscopy performed on the $\{[Mn^{III}(S^{Me2}N_4(6\text{-}Me\text{-}DPEN))]_2(\mu\text{-}O_2)\}^{2+}$ showed resonance-enhanced vibrations at 819 $cm^{-1}$ ($\nu_{O–O}$) and 611 $cm^{-1}$ ($\nu_{Mn–O}$), which were assigned with the help of $^{18}O_2$ isotope-labeling experiments. X-ray-quality crystals of $\{[Mn^{III}(S^{Me2}N_4(6\text{-}Me\text{-}DPEN))]_2(\textit{trans}\text{-}\mu\text{-}1,2\text{-}O_2)(BPh_4)_2\cdot 2CH_3CH_2CN$ were obtained at −80 °C from reaction in propionitrile, and the crystal structure revealed a *trans*-orientation of the two $Mn^{III}$ centers bridged by a μ-1,2-$O_2$ ligand. The O–O bond distance (1.452(5) Å) in the crystal structure was consistent with peroxide formation. The $Mn\cdots N^{Py}$ distances (2.492(3) and 2.410(3) Å) in the crystal structure are significantly longer than the sum of covalent radii of Mn- and N-atoms (2.105 Å). This elongation of the $Mn\cdots N^{Py}$ bonds was attributed to the Jahn–Teller distortions in the $Mn^{III}$ ($d^4$) center and also due to the steric interaction of 6-Me substituents on the pyridine rings with the *gem*-dimethyl groups. Interestingly, dioxygen reactivity of an analogous alkoxide ligated $[Fe^{II}(O^{Me2}N_4(6\text{-}Me\text{-}DPEN))](PF_6)$ complex did not yield an oxo- or peroxo-bridged compound, instead a dihydroxo-bridging $[Fe^{III}(O^{Me2}N_4(6\text{-}Me\text{-}DPEN))]_2(\mu\text{-}OH)_2\text{-}(PF_6)_2$ species was isolated and characterized.[157] Formation of an active $Fe^{IV}(O)$ species was proposed for the reaction, which could abstract a H-atom from the solvent $CH_3CN$ molecule. Isotope labeling experiments with $CD_3CN$ supported this hypothesis. Although successful use of iodosylbenzene in this reaction indicated the intermediacy of an $Fe^{IV}(O)$, no direct evidence for such species could be obtained even at −80 °C.

A high-valent $Mn^{IV}(O)$ complex in which the oxo ligand derives from $O_2$ was synthesized by following the same strategy employed for a related nonheme $Fe^{IV}(O)$ complex (pathway A, Scheme 7).[87,88] The complex $[Mn^{III}H_3buea(O)]^{2-}$ was synthesized by reacting $H_6buea$ and KH with $Mn(OAc)_2$ in the presence of $O_2$.[158,159] Subsequent oxidation of the $Mn^{III}(O)$ complex to a $Mn^{IV}(O)$ complex was achieved by treating $[Mn^{III}H_3buea(O)]^{2-}$ with $[Cp_2Fe]BF_4$.

Recently in 2016, a nonheme mononuclear $Mn^{II}$ complex was shown to perform stepwise oxidation of benzylic C–H bonds with $O_2$ as the oxidant.[160] In an attempt to synthesize $Mn^{II}$ complexes with the dpeo ligand in air, the desired $[Mn^{II}Br_2(dpeo)_2]$ complex was isolated along with the oxidized complex $[Mn^{II}Br_2(hidpe)_2]$ (Scheme 17). The crystal structure of

the $[Mn^{II}Br_2(hidpe)_2]$ complex revealed that the benzylic C–H bonds of the dpeo ligand were converted into a ketone group. An intermediate, two-electron-oxidized $Mn^{III}$(alkoxide) complex $[Mn^{III}(hdpeo)_2]^+$ was also isolated, when $Mn^{II}(ClO_4)_2$ was employed instead of $MnBr_2$. The isolated $[Mn^{III}(hdpeo)_2]^+$ complex was shown to react with $O_2$ to form $[Mn^{II}(hidpeo)_2]^{2+}$, indicating that the alkoxide complex was an intermediate in the overall four-electron oxidation process. Isotope labeling experiments with $^{18}O_2$ and $H_2{}^{18}O$ suggested that $O_2$ was the source of oxygen in the product. A mechanism involving $Mn^{III}(O_2^-)$ and $Mn^{IV}(O)$ intermediates was proposed, but spectroscopic evidence for such intermediates was lacking. The $O_2$-mediated ligand oxidation reaction was specific for $Mn^{2+}$, as it was shown that $Fe^{2+}$, $Ni^{2+}$ or $Zn^{2+}$ were incapable of performing similar C–H oxidation reactions.

## 6. CONCLUSIONS AND PERSPECTIVE

Metalloenzymes that activate dioxygen have highly evolved metal active sites that provide both first- and second-coordination-sphere environments optimized for processing $O_2$. These systems provide a roadmap for the synthetic chemist to prepare small-molecule transition metal complexes that are designed to perform similar $O_2$ activation chemistry. However, it has been challenging to follow this roadmap, because of the subtleties in identifying the key components, and incorporating these structural elements in synthetic ligands for practical use in transition metal chemistry. The chemistry of biomimetic model complexes has relied for a long time on utilizing oxidants other than $O_2$, such as $H_2O_2$ or O-atom transfer agents such as ArIO or organic peracids, to access and study proposed intermediates along the $O_2$ activation pathway. These studies have led to useful information regarding metal–oxo, metal–peroxo and other intermediates, although the direct use of $O_2$ remains a relatively rare occurrence.

In this Perspective, we have provided an overview of the few iron and manganese biomimetic systems that have been employed to carry out $O_2$-mediated oxidation reactions, and that have provided new insights on the mechanism of $O_2$ activation over the past 10 years. Advanced spectroscopic techniques (e.g., rR, Mössbauer, EPR) and low-temperature methods have allowed researchers to trap and spectroscopically characterize key metastable intermediates. Ligand development has also played a crucial role in the activation of $O_2$ at both heme and nonheme metal centers, and has been an essential factor in the subsequent stabilization of the intermediates. It is evident from the nonheme metal studies that dioxygen activation is favored by a high-spin ground state in the starting metal complex. The requirement for high-spin starting complexes suggests that relatively weak-field ligands are more apt to promote $O_2$ reactivity. The ligand also needs to induce an $M^{III}/M^{II}$ (M = Fe, Mn) redox potential that is in a region appropriate for $O_2$ reduction. Significant steric encumbrance of the ligand is another key requirement, crudely mimicking the ability of proteins to sequester the metal active site, and preventing oxo-bridged dimerization and other unwanted bimolecular side-reactions. Second-coordination-sphere effects also need to be controlled, and H-bond donors incorporated into the ligand in the appropriate position can sometimes help to stabilize metal–oxygen species.

Despite $O_2$ activation at Fe or Mn being a prominent target for more than 40 years, there are still relatively few complexes that activate $O_2$ in a rationally designed and controlled manner. From this Perspective, it is evident that $O_2$-activating iron complexes are higher in number than the corresponding manganese complexes, and there are clear opportunities to develop Mn complexes that can utilize $O_2$. The generation and characterization of various metal–oxygen intermediates derived exclusively from $O_2$ remains a challenge for both heme and nonheme systems. There are only three synthetic nonheme iron(III)–superoxide species that have been well characterized, and only two of these come from specific reaction with $O_2$. The latter two species are end-on ($\eta^1$)-bound Fe($O_2^-$) and display electrophilic reactivity toward substrates, while the only side-on ($\eta^2$) superoxide, derived from $KO_2^-$, revealed both electrophilic and nucleophilic reactivity.[161] The differences in reactivity of these Fe($O_2^-$) species are not well understood, and more examples are needed of this fundamental $O_2$ adduct to understand the origins of the different reactivities. Similarly, identifying the M/$O_2$ intermediates involved in substrate oxidation, such as the S-oxygenation reactions described herein, is an important, unmet goal. The *S*-oxygenation reaction is a good example of a highly selective nonheme iron enzyme-mediated reaction that remains challenging to control in a synthetic system.

The use of benign and inexpensive $O_2$ to perform specific and controlled oxidation reactions with the readily available biologically relevant metals Fe and Mn remains a significant challenge for the synthetic chemist. Metalloenzymes can efficiently catalyze $O_2$-dependent oxidations, but their mechanisms of action remain poorly defined in many cases, and advances in synthetic model systems should provide future insights regarding plausible pathways for these transformations. Most of the dioxygen activating biomimetic systems also lack catalytic capability, or their catalytic efficiency is far from the enzymatic scale. Building catalytic reactivity into the synthetic systems with $O_2$ as the oxidant not only would provide systems for comparison with metalloenzymes, but also could provide novel Earth-abundant transition metal catalysts for synthetic transformations.

## Acknowledgments

The NIH (D.P.G., GM101153 and GM119374) is acknowledged for financial support.

## REFERENCES

1. Kovaleva EG, Lipscomb JD. Nat. Chem. Biol. 2008; 4:186–193. [PubMed: 18277980]
2. Wood PM. Biochem. J. 1988; 253:287–289. [PubMed: 2844170]
3. Poulos TL. Chem. Rev. 2014; 114:3919–3962. [PubMed: 24400737]
4. Sono M, Roach MP, Coulter ED, Dawson JH. Chem. Rev. 1996; 96:2841–2888. [PubMed: 11848843]
5. Meunier B, de Visser SP, Shaik S. Chem. Rev. 2004; 104:3947–3980. [PubMed: 15352783]
6. Costas M, Mehn MP, Jensen MP, Que L Jr. Chem. Rev. 2004; 104:939–986. [PubMed: 14871146]
7. Abu-Omar MM, Loaiza A, Hontzeas N. Chem. Rev. 2005; 105:2227–2252. [PubMed: 15941213]
8. Ray K, Pfaff FF, Wang B, Nam W. J. Am. Chem. Soc. 2014; 136:13942–13958. [PubMed: 25215462]
9. Law, NA.; Caudle, MT.; Pecoraro, VL. Advances in Inorganic Chemistry. Sykes, AG., editor. Vol. 46. New York: Academic Press; 1998. p. 305-440.
10. Pecoraro VL, Baldwin MJ, Gelasco A. Chem. Rev. 1994; 94:807–826.

11. Neu HM, Baglia RA, Goldberg DP. Acc. Chem. Res. 2015; 48:2754–2764. [PubMed: 26352344]
12. Nam W. Acc. Chem. Res. 2015; 48:2415–2423. [PubMed: 26203519]
13. Kovacs JA. Acc. Chem. Res. 2015; 48:2744–2753. [PubMed: 26335158]
14. Goldberg DP. Acc. Chem. Res. 2007; 40:626–634. [PubMed: 17580977]
15. Oloo WN, Que L Jr. Acc. Chem. Res. 2015; 48:2612–2621. [PubMed: 26280131]
16. Liu W, Groves JT. Acc. Chem. Res. 2015; 48:1727–1735. [PubMed: 26042637]
17. Cook SA, Borovik AS. Acc. Chem. Res. 2015; 48:2407–2414. [PubMed: 26181849]
18. Ohta T, Liu JG, Naruta Y. Coord. Chem. Rev. 2013; 257:407–413.
19. Kryatov SV, Rybak-Akimova EV, Schindler S. Chem. Rev. 2005; 105:2175–2226. [PubMed: 15941212]
20. Smith LJ, Kahraman A, Thornton JM. Proteins: Struct., Funct., Genet. 2010; 78:2349–2368. [PubMed: 20544970]
21. Groves JT, Nemo TE, Myers RS. J. Am. Chem. Soc. 1979; 101:1032–1033.
22. Che CM, Lo VK, Zhou CY, Huang JS. Chem. Soc. Rev. 2011; 40:1950–1975. [PubMed: 21387046]
23. Groves JT. J. Inorg. Biochem. 2006; 100:434–447. [PubMed: 16516297]
24. Cohen IA, Caughey WS. Biochemistry. 1968; 7:636–641. [PubMed: 5644135]
25. Kao OHW, Wang JH. Biochemistry. 1965; 4:342–347.
26. Balch AL, Chan YW, Cheng RJ, Lamar GN, Latosgrazynski L, Renner MW. J. Am. Chem. Soc. 1984; 106:7779–7785.
27. Chin D-H, Lamar GN, Balch AL. J. Am. Chem. Soc. 1980; 102:5945–5947.
28. Chin D-H, Lamar GN, Balch AL. J. Am. Chem. Soc. 1980; 102:4344–4350.
29. Chin D-H, Balch AL, Lamar GN. J. Am. Chem. Soc. 1980; 102:1446–1448.
30. Takeuchi M, Kodera M, Kano K, Yoshida Z-i. J. Mol. Catal. A: Chem. 1996; 113:51–59.
31. Grinstaff MW, Hill MG, Labinger JA, Gray HB. Science. 1994; 264:1311–1313. [PubMed: 8191283]
32. Ellis PE, Lyons JE. Coord. Chem. Rev. 1990; 105:181–193.
33. Sengupta K, Chatterjee S, Samanta S, Dey A. Proc. Natl. Acad. Sci. U. S. A. 2013; 110:8431–8436. [PubMed: 23650367]
34. Carver CT, Matson BD, Mayer JM. J. Am. Chem. Soc. 2012; 134:5444–5447. [PubMed: 22394189]
35. Costentin C, Dridi H, Savéant J-M. J. Am. Chem. Soc. 2015; 137:13535–13544. [PubMed: 26414306]
36. Collman JP, Devaraj NK, Decréau RA, Yang Y, Yan Y-L, Ebina W, Eberspacher TA, Chidsey CED. Science. 2007; 315:1565–1568. [PubMed: 17363671]
37. Bettelheim A, Kuwana T. Anal. Chem. 1979; 51:2257–2260.
38. Kobayashi N, Nevin WA. Appl. Organomet. Chem. 1996; 10:579–590.
39. Kim E, Helton ME, Wasser IM, Karlin KD, Lu S, Huang HW, Möenne-Loccoz P, Incarvito CD, Rheingold AL, Honecker M, Kaderli S, Zuberbuhler AD. Proc. Natl. Acad. Sci. U. S. A. 2003; 100:3623–3628. [PubMed: 12655050]
40. Ghiladi RA, Kretzer RM, Guzei I, Rheingold AL, Neuhold YM, Hatwell KR, Zuberbuhler AD, Karlin KD. Inorg. Chem. 2001; 40:5754–5767. [PubMed: 11681882]
41. Mittra K, Chatterjee S, Samanta S, Sengupta K, Bhattacharjee H, Dey A. Chem. Commun. 2012; 48:10535–10537.
42. Liu J-G, Ohta T, Yamaguchi S, Ogura T, Sakamoto S, Maeda Y, Naruta Y. Angew. Chem., Int. Ed. 2009; 48:9262–9267.
43. Liu J-G, Shimizu Y, Ohta T, Naruta Y. J. Am. Chem. Soc. 2010; 132:3672–3673. [PubMed: 20196593]
44. Nagaraju P, Ohta T, Liu JG, Ogura T, Naruta Y. Chem. Commun. 2016; 52:7213–7216.
45. Anderson JS, Gallagher AT, Mason JA, Harris TD. J. Am. Chem. Soc. 2014; 136:16489–16492. [PubMed: 25380235]

46. Weschler CJ, Hoffman BM, Basolo F. J. Am. Chem. Soc. 1975; 97:5278–5280. [PubMed: 170324]
47. Hoffman BM, Szymanski T, Brown TG, Basolo F. J. Am. Chem. Soc. 1978; 100:7253–7259.
48. Hoffman BM, Weschler CJ, Basolo F. J. Am. Chem. Soc. 1976; 98:5473–5482. [PubMed: 956568]
49. Moxon NT, Fielding PE, Gregson AK. J. Chem. Soc., Chem. Commun. 1981; 0:98–99.
50. Lever ABP, Wilshire JP, Quan SK. J. Am. Chem. Soc. 1979; 101:3668–3669.
51. Uchida K, Naito S, Soma M, Onishi T, Tamaru K. J. Chem. Soc., Chem. Commun. 1978:217–218.
52. Dismukes GC, Sheats JE, Smegal JA. J. Am. Chem. Soc. 1987; 109:7202–7203.
53. Watanabe T, Ama T, Nakamoto K. Inorg. Chem. 1983; 22:2470–2472.
54. Battioni P, Bartoli JF, Leduc P, Fontecave M, Mansuy D. J. Chem. Soc., Chem. Commun. 1987:791–792.
55. Sakurai H, Mori Y, Shibuya M. Inorg. Chim. Acta. 1989; 162:23–25.
56. Jung J, Neu HM, Leeladee P, Siegler MA, Ohkubo K, Goldberg DP, Fukuzumi S. Inorg. Chem. 2016; 55:3218–3228. [PubMed: 26974004]
57. Neu HM, Jung J, Baglia RA, Siegler MA, Ohkubo K, Fukuzumi S, Goldberg DP. J. Am. Chem. Soc. 2015; 137:4614–4617. [PubMed: 25839905]
58. Prokop KA, Goldberg DP. J. Am. Chem. Soc. 2012; 134:8014–8017. [PubMed: 22533822]
59. Zaragoza JPT, Siegler MA, Goldberg DP. Chem. Commun. 2016; 52:167–170.
60. Jung J, Ohkubo K, Prokop-Prigge KA, Neu HM, Goldberg DP, Fukuzumi S. Inorg. Chem. 2013; 52:13594–13604. [PubMed: 24219426]
61. Jung J, Ohkubo K, Goldberg DP, Fukuzumi S. J. Phys. Chem. A. 2014; 118:6223–6229. [PubMed: 25079061]
62. Cho K, Leeladee P, McGown AJ, DeBeer S, Goldberg DP. J. Am. Chem. Soc. 2012; 134:7392–7399. [PubMed: 22489757]
63. McGown AJ, Kerber WD, Fujii H, Goldberg DP. J. Am. Chem. Soc. 2009; 131:8040–8048. [PubMed: 19462977]
64. Liu H-Y, Mahmood MHR, Qiu S-X, Chang CK. Coord. Chem. Rev. 2013; 257:1306–1333.
65. Schwalbe M, Dogutan DK, Stoian SA, Teets TS, Nocera DG. Inorg. Chem. 2011; 50:1368–1377. [PubMed: 21244031]
66. Simkhovich L, Goldberg I, Gross Z. Inorg. Chem. 2002; 41:5433–5439. [PubMed: 12377038]
67. Vogel E, Will S, Tilling AS, Neumann L, Lex J, Bill E, Trautwein AX, Wieghardt K. Angew. Chem., Int. Ed. Engl. 1994; 33:731–735.
68. Solomon EI, Light KM, Liu LV, Srnec M, Wong SD. Acc. Chem. Res. 2013; 46:2725–2739. [PubMed: 24070107]
69. Bruijnincx PCA, van Koten G, Klein Gebbink RJM. Chem. Soc. Rev. 2008; 37:2716–2744. [PubMed: 19020684]
70. Xing G, Diao Y, Hoffart LM, Barr EW, Prabhu KS, Arner RJ, Reddy CC, Krebs C, Bollinger JM Jr. Proc. Natl. Acad. Sci. U. S. A. 2006; 103:6130–6135. [PubMed: 16606846]
71. Schatz M, Raab V, Foxon SP, Brehm G, Schneider S, Reiher M, Holthausen MC, Sundermeyer J, Schindler S. Angew. Chem., Int. Ed. 2004; 43:4360–4363.
72. Peterson RL, Himes RA, Kotani H, Suenobu T, Tian L, Siegler MA, Solomon EI, Fukuzumi S, Karlin KD. J. Am. Chem. Soc. 2011; 133:1702–1705. [PubMed: 21265534]
73. Cho J, Woo J, Nam W. J. Am. Chem. Soc. 2010; 132:5958–5959. [PubMed: 20392047]
74. Cho J, Kang HY, Liu LV, Sarangi R, Solomon EI, Nam W. Chem. Sci. 2013; 4:1502–1508. [PubMed: 23662168]
75. Qin K, Incarvito CD, Rheingold AL, Theopold KH. Angew. Chem., Int. Ed. 2002; 41:2333–2335.
76. Shan X, Que L Jr. Proc. Natl. Acad. Sci. U. S. A. 2005; 102:5340–5345. [PubMed: 15802473]
77. Chiang CW, Kleespies ST, Stout HD, Meier KK, Li P-Y, Bominaar EL, Que L Jr, Münck E, Lee WZ. J. Am. Chem. Soc. 2014; 136:10846–10849. [PubMed: 25036460]
78. Stout HD, Kleespies ST, Chiang C-W, Lee W-Z, Que L, Münck E, Bominaar EL. Inorg. Chem. 2016; 55:5215–5226. [PubMed: 27159412]

79. Oddon F, Chiba Y, Nakazawa J, Ohta T, Ogura T, Hikichi S. Angew. Chem., Int. Ed. 2015; 54:7336–7339.
80. Price JC, Barr EW, Tirupati B, Bollinger JM Jr, Krebs C. Biochemistry. 2003; 42:7497–7508. [PubMed: 12809506]
81. Krebs C, Fujimori DG, Walsh CT, Bollinger JM Jr. Acc. Chem. Res. 2007; 40:484–492. [PubMed: 17542550]
82. Hoffart LM, Barr EW, Guyer RB, Bollinger JM Jr, Krebs C. Proc. Natl. Acad. Sci. U. S. A. 2006; 103:14738–14743. [PubMed: 17003127]
83. Matthews ML, Krest CM, Barr EW, Vaillancourt FH, Walsh CT, Green MT, Krebs C, Bollinger JM Jr. Biochemistry. 2009; 48:4331–4343. [PubMed: 19245217]
84. Fujimori DG, Barr EW, Matthews ML, Koch GM, Yonce JR, Walsh CT, Bollinger JM Jr, Krebs C, Riggs-Gelasco PJ. J. Am. Chem. Soc. 2007; 129:13408–13409. [PubMed: 17939667]
85. Eser BE, Barr EW, Frantom PA, Saleh L, Bollinger JM Jr, Krebs C, Fitzpatrick PF. J. Am. Chem. Soc. 2007; 129:11334–11335. [PubMed: 17715926]
86. Panay AJ, Lee M, Krebs C, Bollinger JM Jr, Fitzpatrick PF. Biochemistry. 2011; 50:1928–1933. [PubMed: 21261288]
87. MacBeth CE, Golombek AP, Young VG Jr, Yang C, Kuczera K, Hendrich MP, Borovik AS. Science. 2000; 289:938–941. [PubMed: 10937994]
88. Lacy DC, Gupta R, Stone KL, Greaves J, Ziller JW, Hendrich MP, Borovik AS. J. Am. Chem. Soc. 2010; 132:12188–12190. [PubMed: 20704272]
89. Bigi JP, Harman WH, Lassalle-Kaiser B, Robles DM, Stich TA, Yano J, Britt RD, Chang CJ. J. Am. Chem. Soc. 2012; 134:1536–1542. [PubMed: 22214221]
90. Biswas AN, Puri M, Meier KK, Oloo WN, Rohde GT, Bominaar EL, Münck E, Que L Jr. J. Am. Chem. Soc. 2015; 137:2428–2431. [PubMed: 25674662]
91. England J, Martinho M, Farquhar ER, Frisch JR, Bominaar EL, Münck E, Que L Jr. Angew. Chem., Int. Ed. 2009; 48:3622–3626.
92. Puri M, Que L Jr. Acc. Chem. Res. 2015; 48:2443–2452. [PubMed: 26176555]
93. Puri M, Biswas AN, Fan R, Guo Y, Que L Jr. J. Am. Chem. Soc. 2016; 138:2484–2487. [PubMed: 26875530]
94. Kim SO, Sastri CV, Seo MS, Kim J, Nam W. J. Am. Chem. Soc. 2005; 127:4178–4179. [PubMed: 15783193]
95. Rohde J-U, In JH, Lim MH, Brennessel WW, Bukowski MR, Stubna A, Münck E, Nam W, Que L Jr. Science. 2003; 299:1037–1039. [PubMed: 12586936]
96. Thibon A, England J, Martinho M, Young VG Jr, Frisch JR, Guillot R, Girerd JJ, Münck E, Que L Jr, Banse F. Angew. Chem., Int. Ed. 2008; 47:7064–7067.
97. Park H, Bittner MM, Baus JS, Lindeman SV, Fiedler AT. Inorg. Chem. 2012; 51:10279–10289. [PubMed: 22974346]
98. Hong S, Lee YM, Shin W, Fukuzumi S, Nam W. J. Am. Chem. Soc. 2009; 131:13910–13911. [PubMed: 19746912]
99. Martinho M, Blain G, Banse F. Dalton Trans. 2010; 39:1630–1634. [PubMed: 20104327]
100. Li F, Van Heuvelen KM, Meier KK, Münck E, Que L Jr. J. Am. Chem. Soc. 2013; 135:10198–10201. [PubMed: 23802702]
101. Nishida Y, Lee Y-M, Nam W, Fukuzumi S. J. Am. Chem. Soc. 2014; 136:8042–8049. [PubMed: 24809677]
102. Lee YM, Hong S, Morimoto Y, Shin W, Fukuzumi S, Nam W. J. Am. Chem. Soc. 2010; 132:10668–10670. [PubMed: 20681694]
103. Ségaud N, Anxolabéhère-Mallart E, Sénéchal-David K, Acosta-Rueda L, Robert M, Banse F. Chem. Sci. 2015; 6:639–647.
104. Kishima T, Matsumoto T, Nakai H, Hayami S, Ohta T, Ogo S. Angew. Chem., Int. Ed. 2016; 55:724–727.
105. Cho J, Sarangi R, Kang HY, Lee JY, Kubo M, Ogura T, Solomon EI, Nam W. J. Am. Chem. Soc. 2010; 132:16977–16986. [PubMed: 21062059]

106. Cho J, Sarangi R, Annaraj J, Kim SY, Kubo M, Ogura T, Solomon EI, Nam W. Nat. Chem. 2009; 1:568–572. [PubMed: 20711413]
107. Seo MS, Kim JY, Annaraj J, Kim Y, Lee Y-M, Kim S-J, Kim J, Nam W. Angew. Chem., Int. Ed. 2007; 46:377–380.
108. Karlsson A, Parales JV, Parales RE, Gibson DT, Eklund H, Ramaswamy S. Science. 2003; 299:1039–1042. [PubMed: 12586937]
109. Cho J, Jeon S, Wilson SA, Liu LV, Kang EA, Braymer JJ, Lim MH, Hedman B, Hodgson KO, Valentine JS, Solomon EI, Nam W. Nature. 2011; 478:502–505. [PubMed: 22031443]
110. McDonald AR, Que L Jr. Coord. Chem. Rev. 2013; 257:414–428.
111. Bruijnincx PCA, Lutz M, Spek AL, Hagen WR, Weckhuysen BM, van Koten G, Gebbink RJM. J. Am. Chem. Soc. 2007; 129:2275–2286. [PubMed: 17266307]
112. Chakraborty B, Bhunya S, Paul A, Paine TK. Inorg. Chem. 2014; 53:4899–4912. [PubMed: 24787025]
113. Jo DH, Que L Jr. Angew. Chem., Int. Ed. 2000; 39:4284–4287.
114. Bugg TDH, Lin G. Chem. Commun. 2001:941–952.
115. Bruijnincx PCA, Lutz M, Spek AL, Hagen WR, van Koten G, Gebbink RJM. Inorg. Chem. 2007; 46:8391–8402. [PubMed: 17722878]
116. Mayilmurugan R, Stoeckli-Evans H, Palaniandavar M. Inorg. Chem. 2008; 47:6645–6658. [PubMed: 18597419]
117. Váradi T, Pap JS, Giorgi M, Párkányi L, Csay T, Speier G, Kaizer J. Inorg. Chem. 2013; 52:1559–1569. [PubMed: 23320898]
118. Chatterjee S, Paine TK. Inorg. Chem. 2015; 54:1720–1727. [PubMed: 25646806]
119. Chakraborty B, Paine TK. Angew. Chem., Int. Ed. 2013; 52:920–924.
120. Bittner MM, Lindeman SV, Popescu CV, Fiedler AT. Inorg. Chem. 2014; 53:4047–4061. [PubMed: 24697567]
121. Bittner MM, Lindeman SV, Fiedler AT. J. Am. Chem. Soc. 2012; 134:5460–5463. [PubMed: 22417231]
122. Hausinger RP. Crit. Rev. Biochem. Mol. Biol. 2004; 39:21–68. [PubMed: 15121720]
123. Wong SD, Srnec M, Matthews ML, Liu LV, Kwak Y, Park K, Bell CB III, Alp EE, Zhao J, Yoda Y, Kitao S, Seto M, Krebs C, Bollinger JM Jr, Solomon EI. Nature. 2013; 499:320–323. [PubMed: 23868262]
124. Ha EH, Ho RYN, Kisiel JF, Valentine JS. Inorg. Chem. 1995; 34:2265–2266.
125. Mehn MP, Fujisawa K, Hegg EL, Que L Jr. J. Am. Chem. Soc. 2003; 125:7828–7842. [PubMed: 12823001]
126. Hegg EL, Ho RYN, Que L Jr. J. Am. Chem. Soc. 1999; 121:1972–1973.
127. Mukherjee A, Martinho M, Bominaar EL, Münck E, Que L Jr. Angew. Chem., Int. Ed. 2009; 48:1780–1783.
128. Chatterjee S, Paine TK. Angew. Chem., Int. Ed. 2016; 55:7717–7722.
129. Chatterjee S, Paine TK. Angew. Chem., Int. Ed. 2015; 54:9338–9342.
130. Paria S, Chatterjee S, Paine TK. Inorg. Chem. 2014; 53:2810–2821. [PubMed: 24627956]
131. Paria S, Que L Jr, Paine TK. Angew. Chem., Int. Ed. 2011; 50:11129–11132.
132. Paine TK, Paria S, Que L Jr. Chem. Commun. 2010; 46:1830–1832.
133. Pojer F, Kahlich R, Kammerer B, Li SM, Heide L. J. Biol. Chem. 2003; 278:30661–30668. [PubMed: 12777382]
134. McQuilken AC, Goldberg DP. Dalton Trans. 2012; 41:10883–10899. [PubMed: 22814765]
135. Kumar D, Thiel W, de Visser SP. J. Am. Chem. Soc. 2011; 133:3869–3882. [PubMed: 21344861]
136. Ye S, Wu X, Wei L, Tang D, Sun P, Bartlam M, Rao Z. J. Biol. Chem. 2007; 282:3391–3402. [PubMed: 17135237]
137. Pierce BS, Gardner JD, Bailey LJ, Brunold TC, Fox BG. Biochemistry. 2007; 46:8569–8578. [PubMed: 17602574]
138. Simmons CR, Liu Q, Huang Q, Hao Q, Begley TP, Karplus PA, Stipanuk MH. J. Biol. Chem. 2006; 281:18723–18733. [PubMed: 16611640]

139. McCoy JG, Bailey LJ, Bitto E, Bingman CA, Aceti DJ, Fox BG, Phillips GN Jr. Proc. Natl. Acad. Sci. U. S. A. 2006; 103:3084–3089. [PubMed: 16492780]
140. Jiang Y, Widger LR, Kasper GD, Siegler MA, Goldberg DP. J. Am. Chem. Soc. 2010; 132:12214–12215. [PubMed: 20712312]
141. Badiei YM, Siegler MA, Goldberg DP. J. Am. Chem. Soc. 2011; 133:1274–1277. [PubMed: 21207980]
142. McQuilken AC, Jiang Y, Siegler MA, Goldberg DP. J. Am. Chem. Soc. 2012; 134:8758–8761. [PubMed: 22578255]
143. Sallmann M, Siewert I, Fohlmeister L, Limberg C, Knispel C. Angew. Chem., Int. Ed. 2012; 51:2234–2237.
144. Sallmann M, Braun B, Limberg C. Chem. Commun. 2015; 51:6785–6787.
145. Cho J, Woo J, Nam W. J. Am. Chem. Soc. 2012; 134:11112–11115. [PubMed: 22713134]
146. Mabad B, Tuchagues JP, Hwang YT, Hendrickson DN. J. Am. Chem. Soc. 1985; 107:2801–2802.
147. Coleman WM, Taylor LT. Inorg. Chim. Acta. 1978; 30:L291–L293.
148. Kipke CA, Scott MJ, Gohdes JW, Armstrong WH. Inorg. Chem. 1990; 29:2193–2194.
149. Kitajima N, Singh UP, Amagai H, Osawa M, Morooka Y. J. Am. Chem. Soc. 1991; 113:7757–7758.
150. Bossek U, Weyhermüller T, Wieghardt K, Nuber B, Weiss J. J. Am. Chem. Soc. 1990; 112:6387–6388.
151. Bhula R, Gainsford GJ, Weatherburn DC. J. Am. Chem. Soc. 1988; 110:7550–7552.
152. Frederick FC, Taylor LT. Polyhedron. 1986; 5:887–893.
153. Liu L-L, Li H-X, Wan L-M, Ren Z-G, Wang H-F, Lang J-P. Chem. Commun. 2011; 47:11146–11148.
154. Shook RL, Gunderson WA, Greaves J, Ziller JW, Hendrich MP, Borovik AS. J. Am. Chem. Soc. 2008; 130:8888–8889. [PubMed: 18570414]
155. Shook RL, Peterson SM, Greaves J, Moore C, Rheingold AL, Borovik AS. J. Am. Chem. Soc. 2011; 133:5810–5817. [PubMed: 21425844]
156. Coggins MK, Sun X, Kwak Y, Solomon EI, Rybak-Akimova E, Kovacs JA. J. Am. Chem. Soc. 2013; 135:5631–5640. [PubMed: 23470101]
157. Coggins MK, Toledo S, Kovacs JA. Inorg. Chem. 2013; 52:13325–13331. [PubMed: 24229319]
158. Parsell TH, Behan RK, Green MT, Hendrich MP, Borovik AS. J. Am. Chem. Soc. 2006; 128:8728–8729. [PubMed: 16819856]
159. MacBeth CE, Gupta R, Mitchell-Koch KR, Young VG Jr, Lushington GH, Thompson WH, Hendrich MP, Borovik AS. J. Am. Chem. Soc. 2004; 126:2556–2567. [PubMed: 14982465]
160. Deville C, Padamati SK, Sundberg J, McKee V, Browne WR, McKenzie C. J. Angew. Chem., Int. Ed. 2016; 55:545–549.
161. Hong S, Sutherlin KD, Park J, Kwon E, Siegler MA, Solomon EI, Nam W. Nat. Commun. 2014; 5:5440. [PubMed: 25510711]

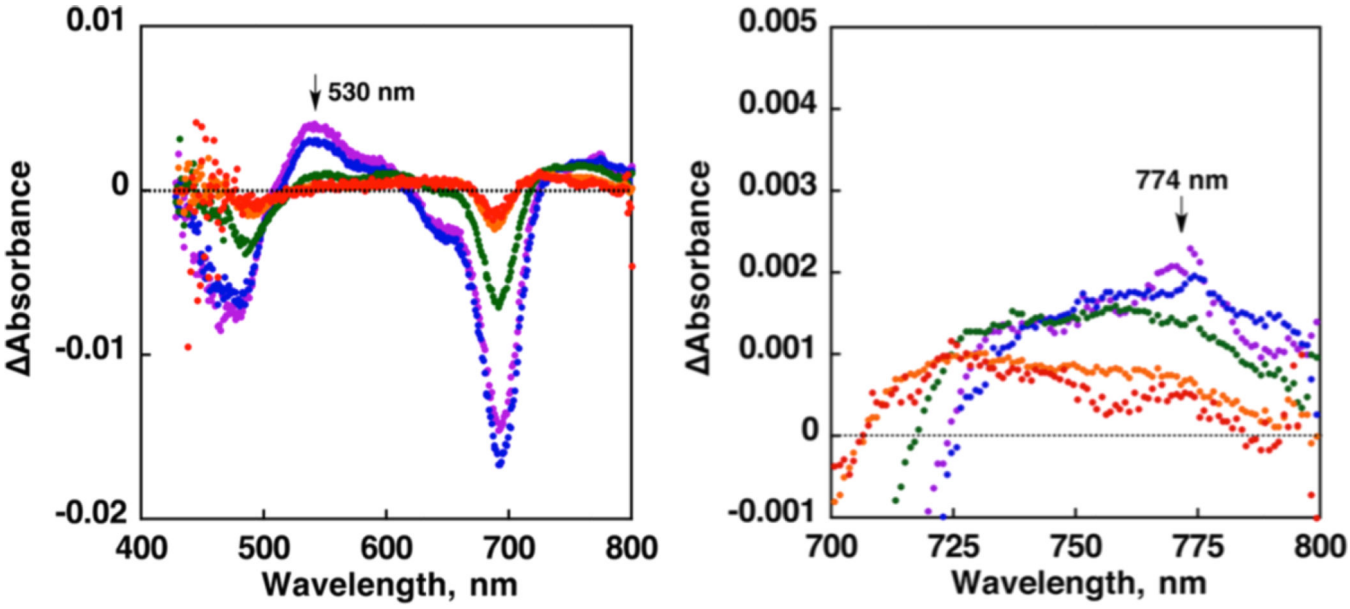


**Figure 1.**

Transient absorption spectral changes of the [$(TBP_8Cz)Mn^{III}$]* ($^5T_1$) (530 nm) and [$(TBP_8Cz)Mn^{III}$]* ($^7T_1$) (774 nm) states, generated from photoexcitation of $(TBP_8Cz)Mn^{III}$ in benzonitrile. Reprinted with permission from ref 60. Copyright 2013 American Chemical Society.

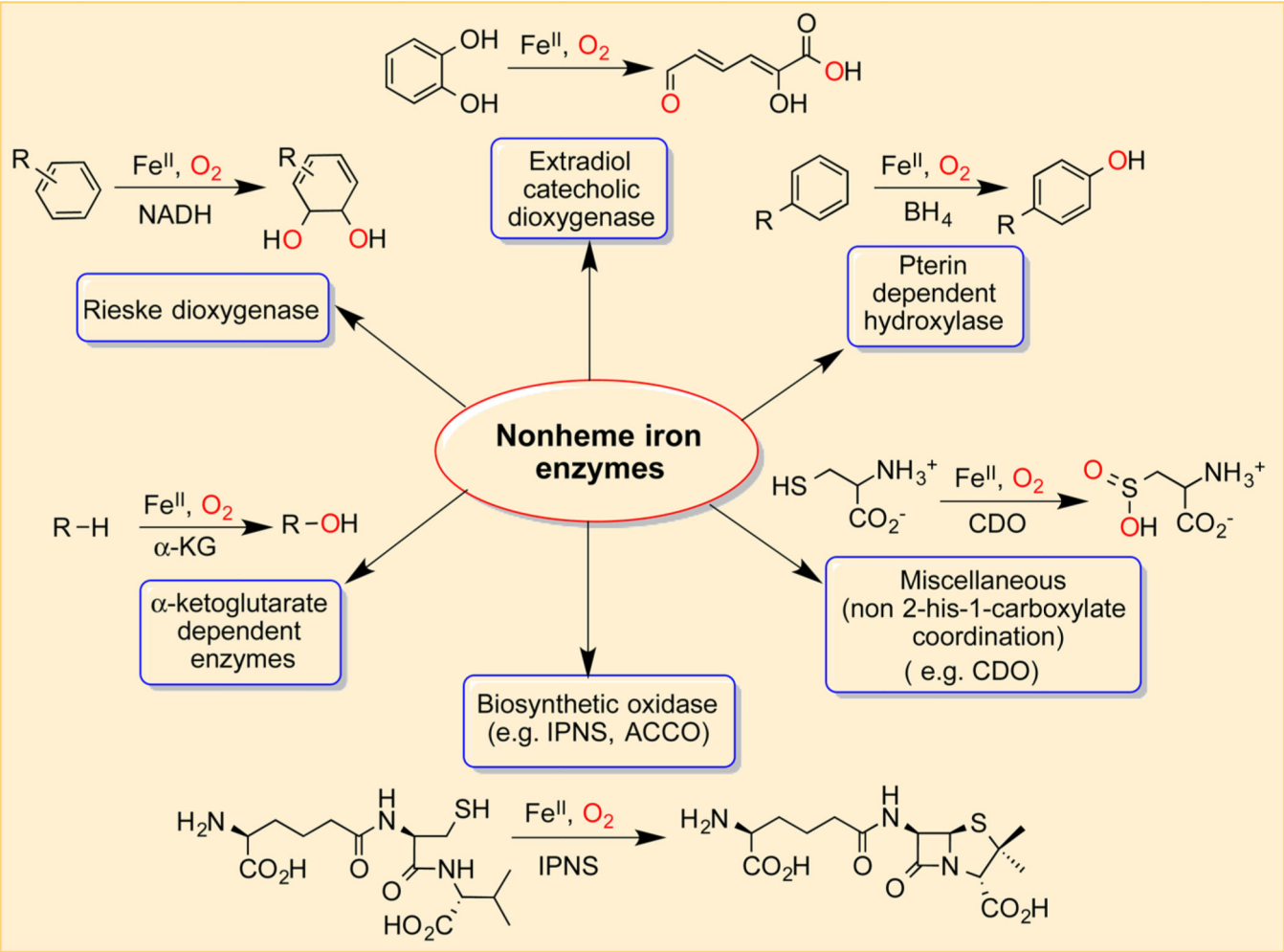


**Figure 2.**

Nonheme iron enzymes and the various transformations that they catalyze. Adapted with permission from ref 1. Copyright 2008 Macmillan Publishers Ltd.

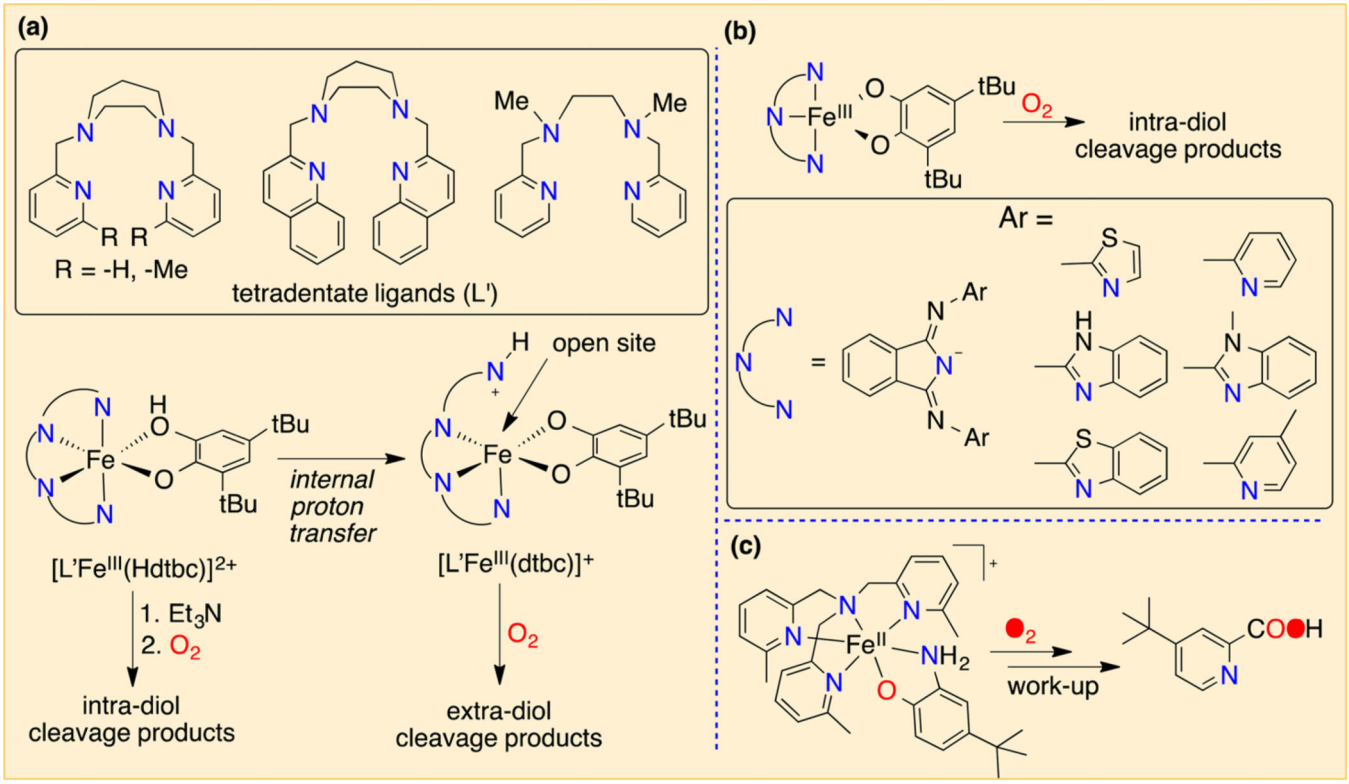


**Figure 3.**

(a) Tetradentate N4 ligands and dioxygenase reactivity for the corresponding mono- and doubly deprotonated catechol complexes. (b) Dioxygenase reactivity for $Fe^{III}$–catecholate complexes with tridentate N3 ligands. (c) Reaction of iron(II)–aminophenolate complex with dioxygen. Adapted with permissions from refs 116, 117, and 119. Copyright 2008 American Chemical Society, Copyright 2013 American Chemical Society, and Copyright 2014 American Chemical Society.

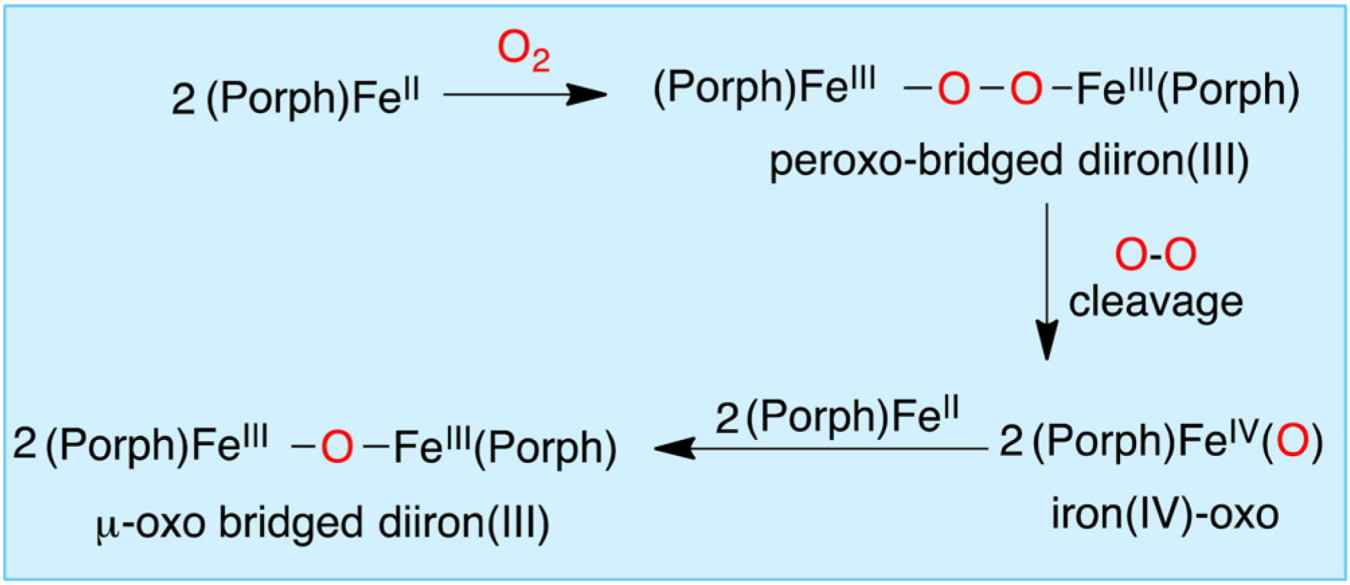


**Scheme 1.**
Dioxygen-Mediated Autoxidation Mechanism for Ferrous–Porphyrin Complexes

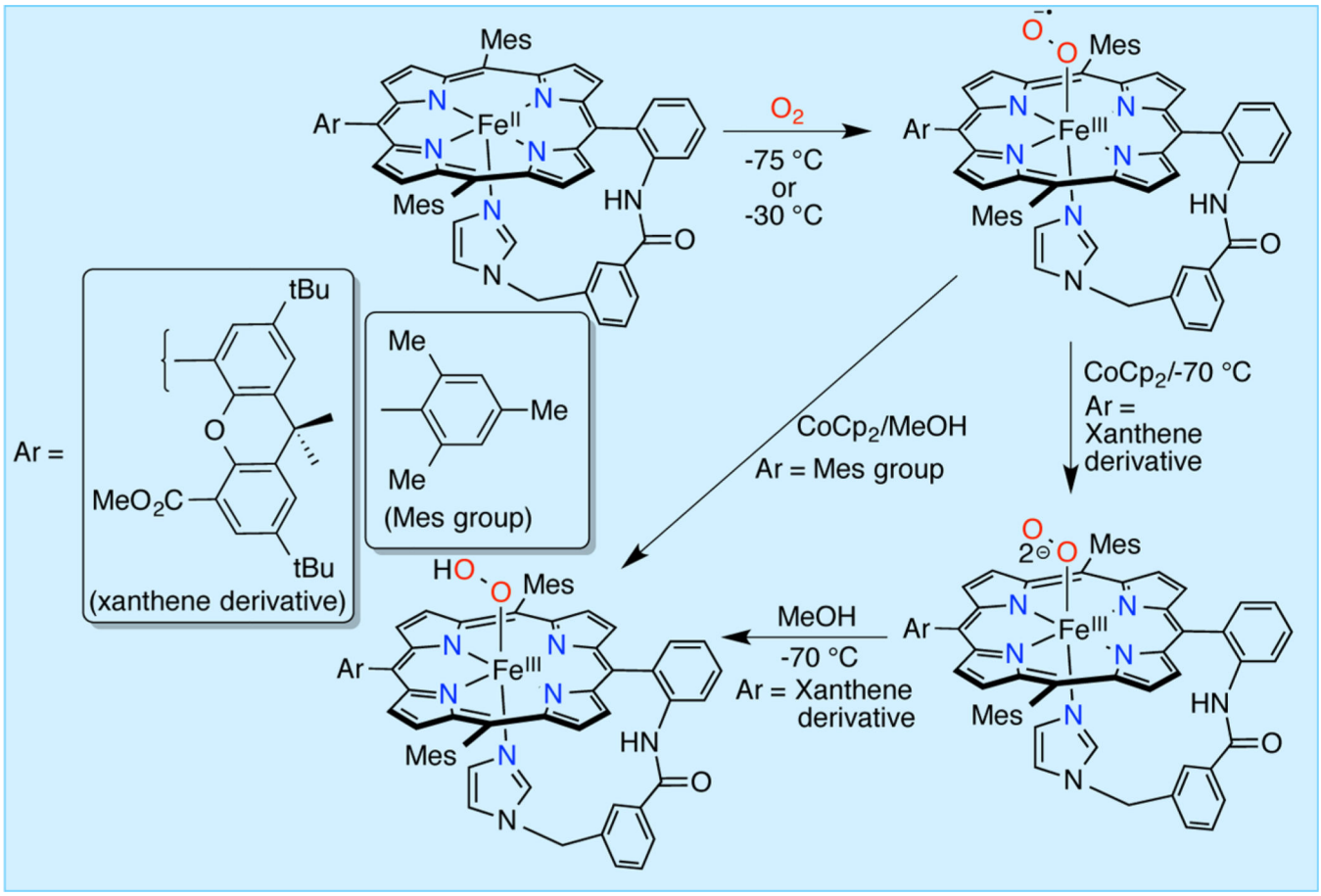


**Scheme 2.**

Formation of an $Fe^{III}(O_2^{-})$ Species Generated from the Reaction of Ferrous–Porphyrin with $O_2$, and the One-Electron Reduction of the $Fe^{III}(O_2^{-})$ Complex[a]

[a]Adapted with permission from refs 42 and 43. Copyright 2009 John Wiley & Sons, Inc., and Copyright 2010 American Chemical Society.

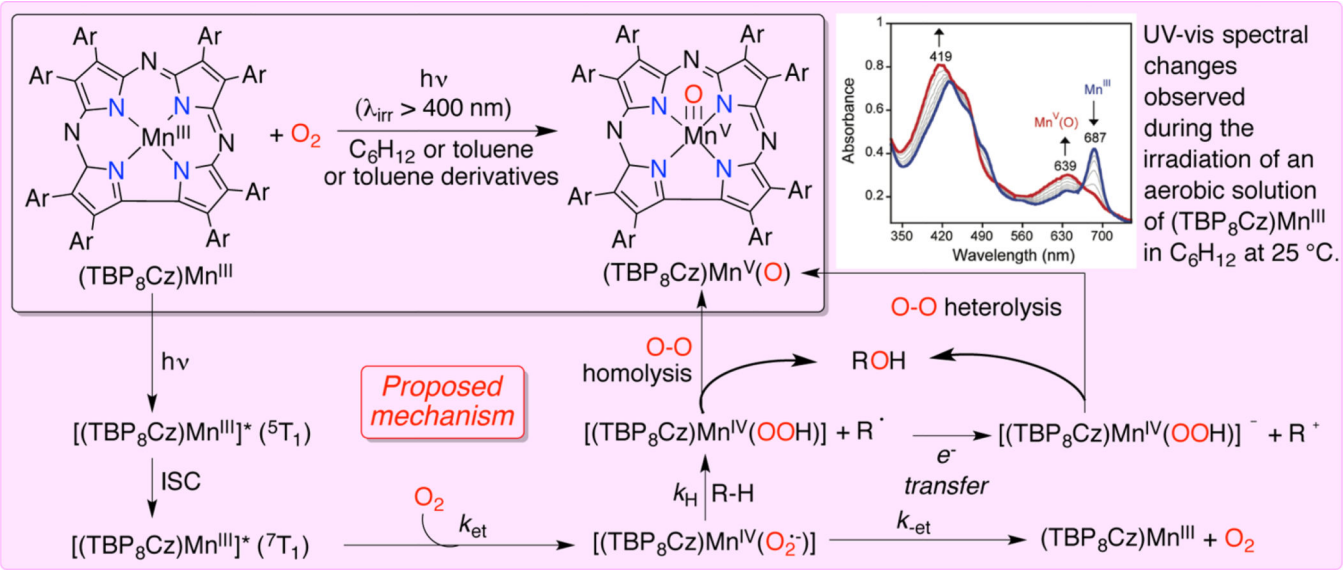


**Scheme 3.**

Photoinitiated Dioxygen Activation by a $Mn^{III}$–Corrolazine Complex and the Mechanism of Formation of a $Mn^{V}(O)$ Species[a]

[a]Adapted with permission from refs 58 and 60. Copyright 2012 American Chemical Society, and Copyright 2013 American Chemical Society.

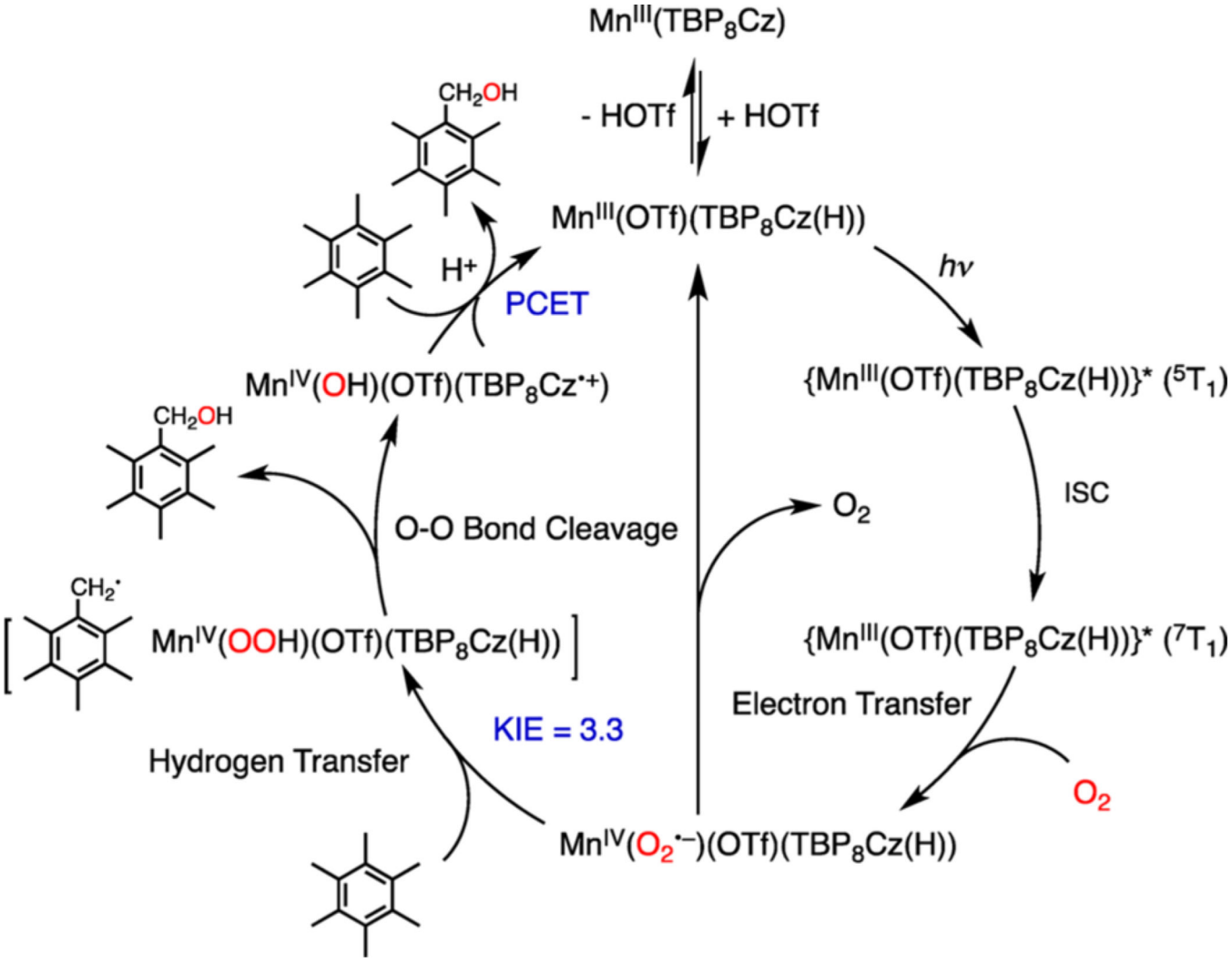


**Scheme 4.**

Proposed Mechanism for the Acid-Assisted Catalytic Oxidation of Hexamethyl Benzene[a]

[a]Reprinted with permission from ref 56. Copyright 2016 American Chemical Society.

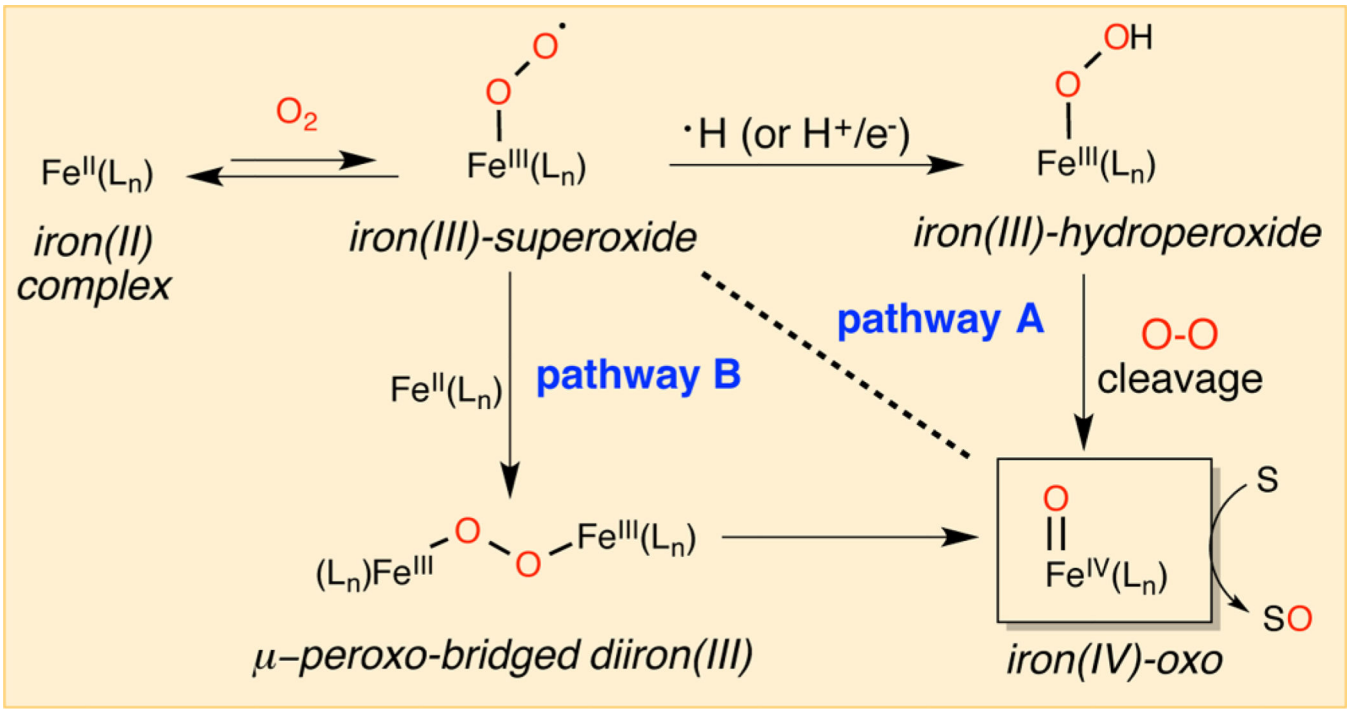


**Scheme 5.**
Proposed Dioxygen Activation Pathways for Synthetic Nonheme Iron Complexes

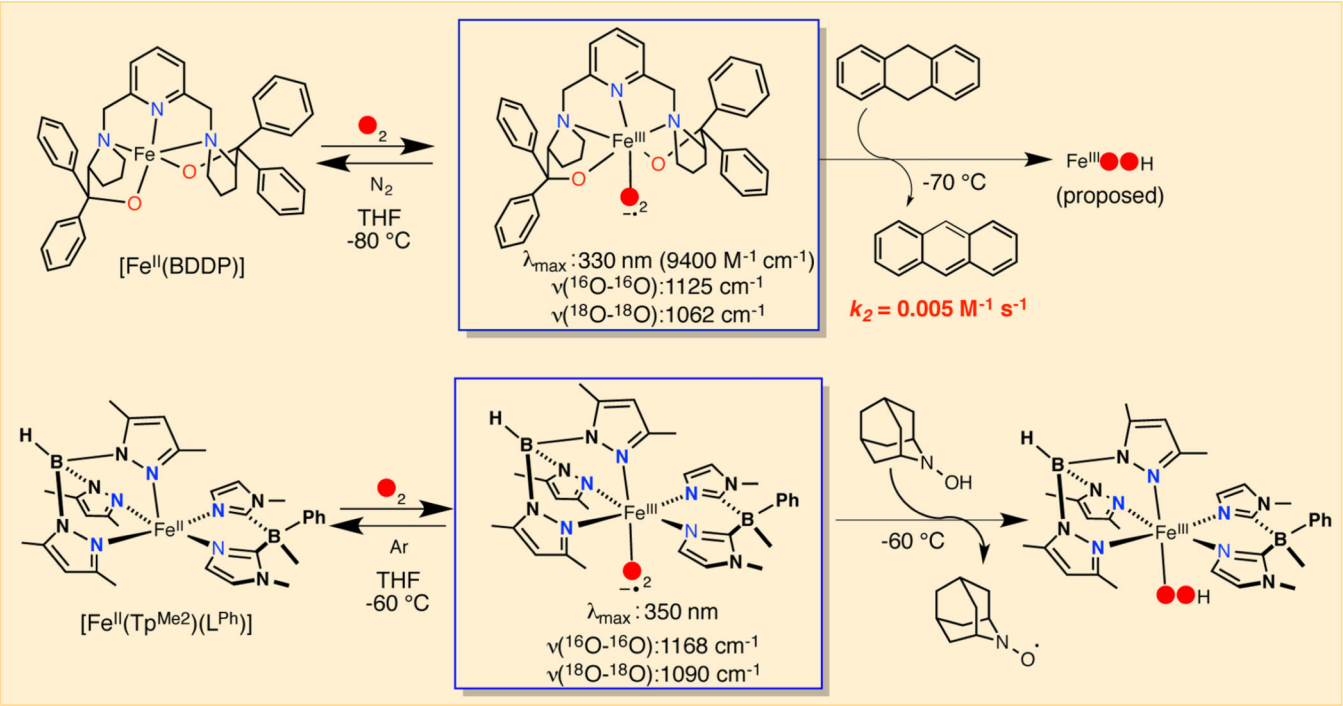


**Scheme 6.**

Formation and Reactivity of the $[Fe^{III}(O_2^{-})(BDDP)]$ (Top) and $[Fe^{III}(O_2^{-})(Tp^{Me2})(L^{Ph})]$ (Bottom) Complexes[a]

[a]Bottom panel adapted with permission from ref 79. Copyright 2015 John Wiley & Sons, Inc.

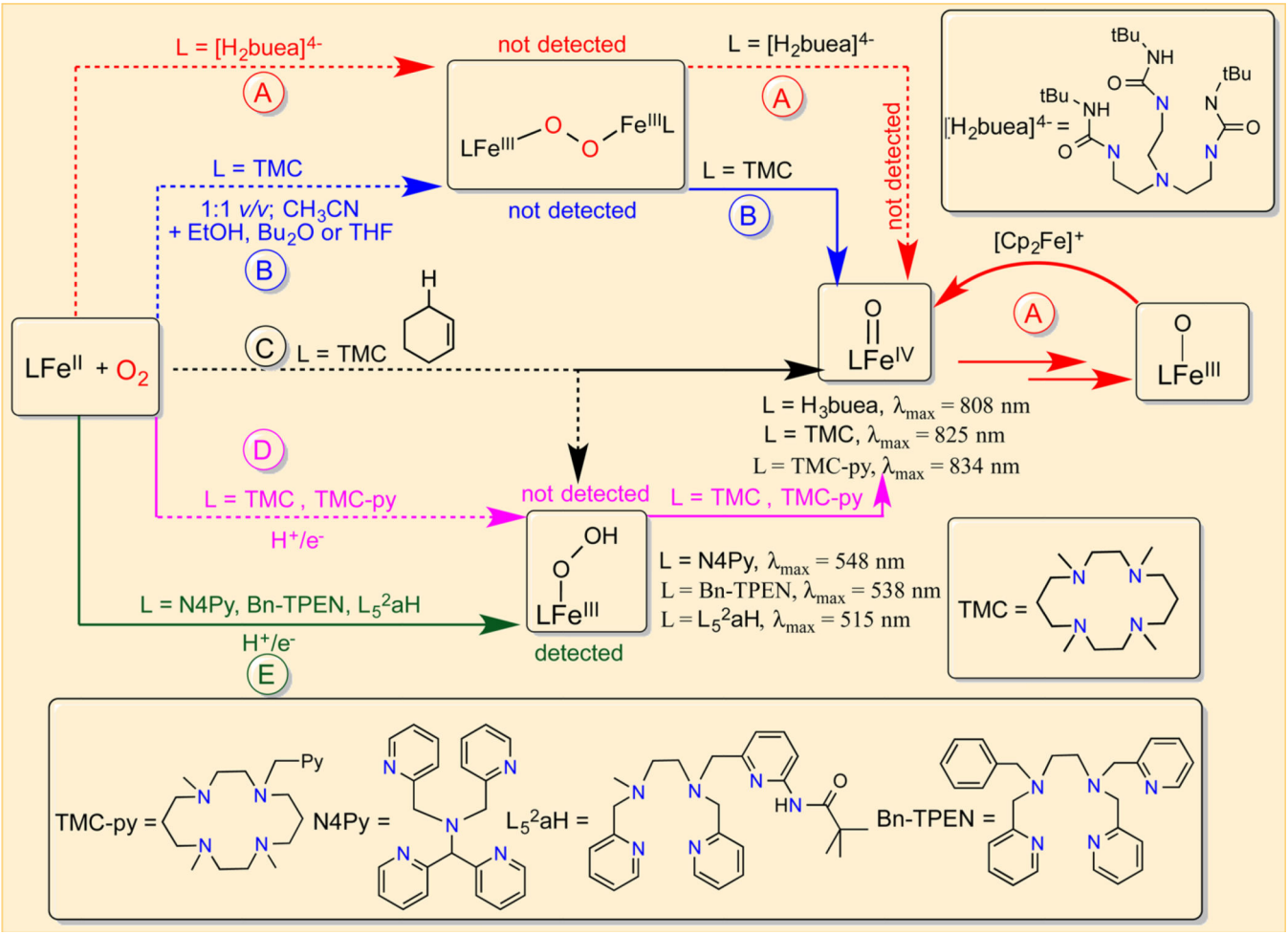


**Scheme 7.**

Formation of Nonheme Iron(III)–Peroxo and Iron(IV)–Oxo Complexes Derived from the Reaction of $Fe^{II}$ Complexes and $O_2$[a]

[a]Dotted arrows indicate formation of a proposed but nondetected intermediate, and solid arrows indicate that the species was detected spectroscopically characterized.

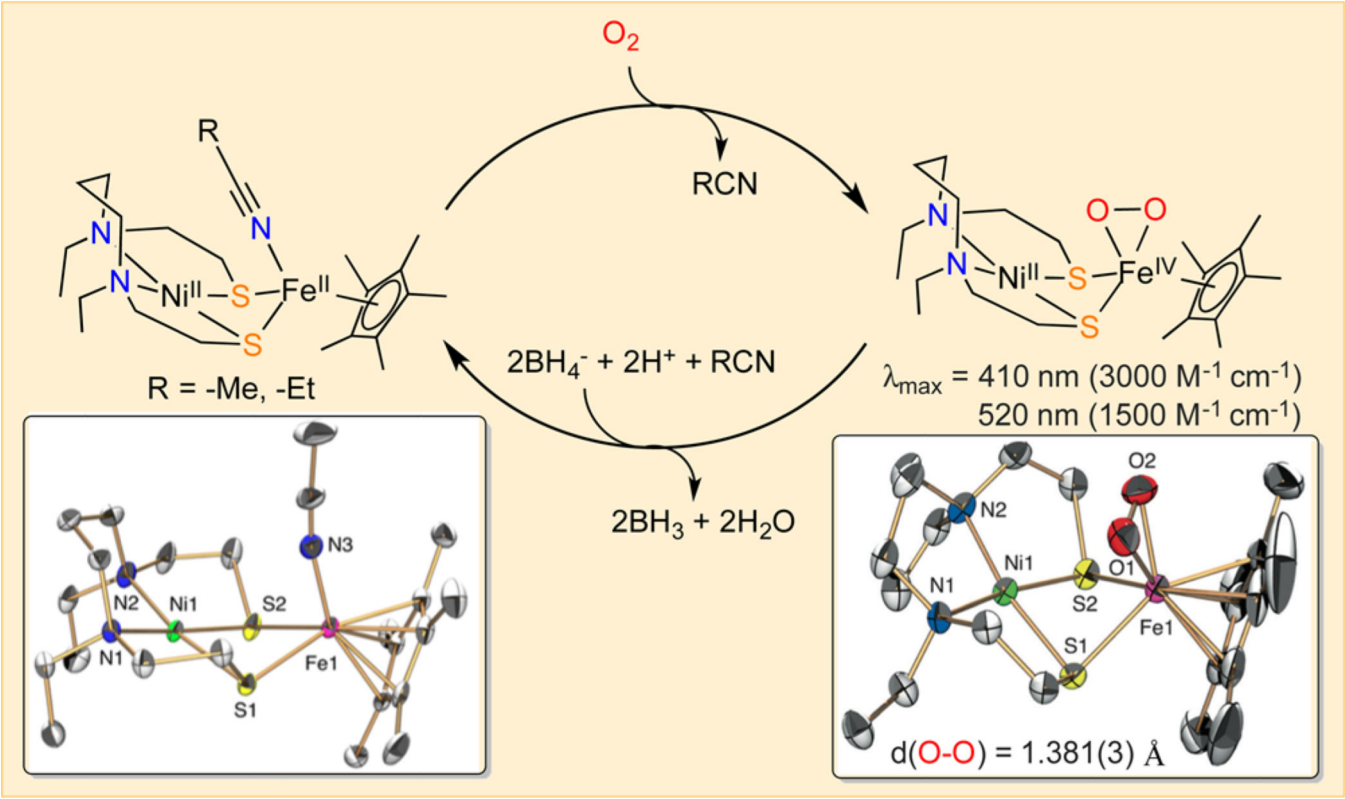


**Scheme 8.**

$O_2$ Activation by [$Ni^{II}Fe^{II}$] Complexes (Crystal Structure, Bottom Left) To Form an $Fe^{IV}(O_2^{2-})$ Species (Crystal Structure, Bottom Right) and Subsequent $2e^-$ Reduction To Generate $H_2O$[a]

[a]Adapted with permission from ref 104. Copyright 2016 John Wiley & Sons, Inc.

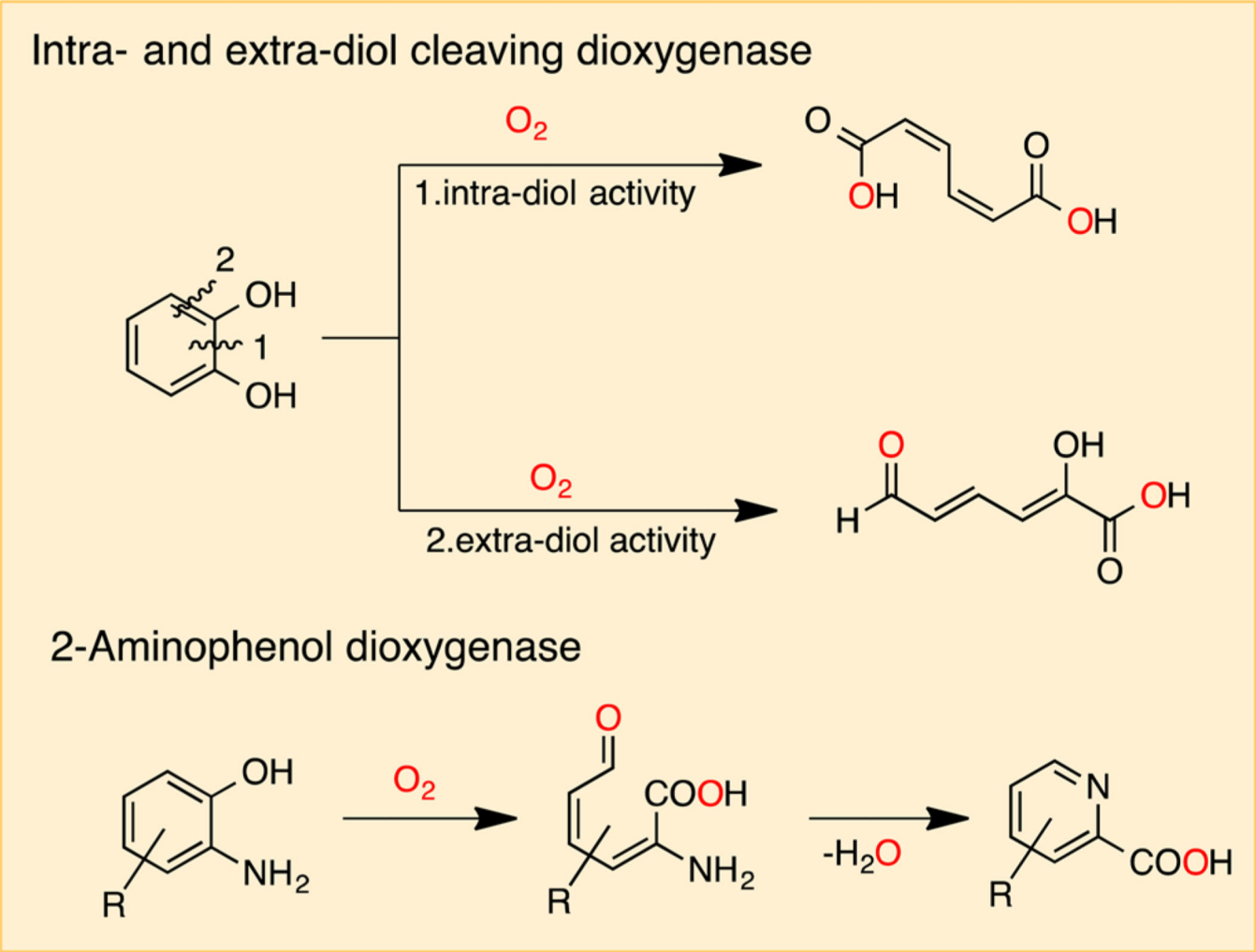


**Scheme 9.**

Reactions Catalyzed by Intra- and Extradiol Cleaving and 2-Aminophenol Dioxygenases[a]

[a]Reprinted with permission from refs 111 and 112. Copyright 2007 American Chemical Society, and Copyright 2014 American Chemical Society.

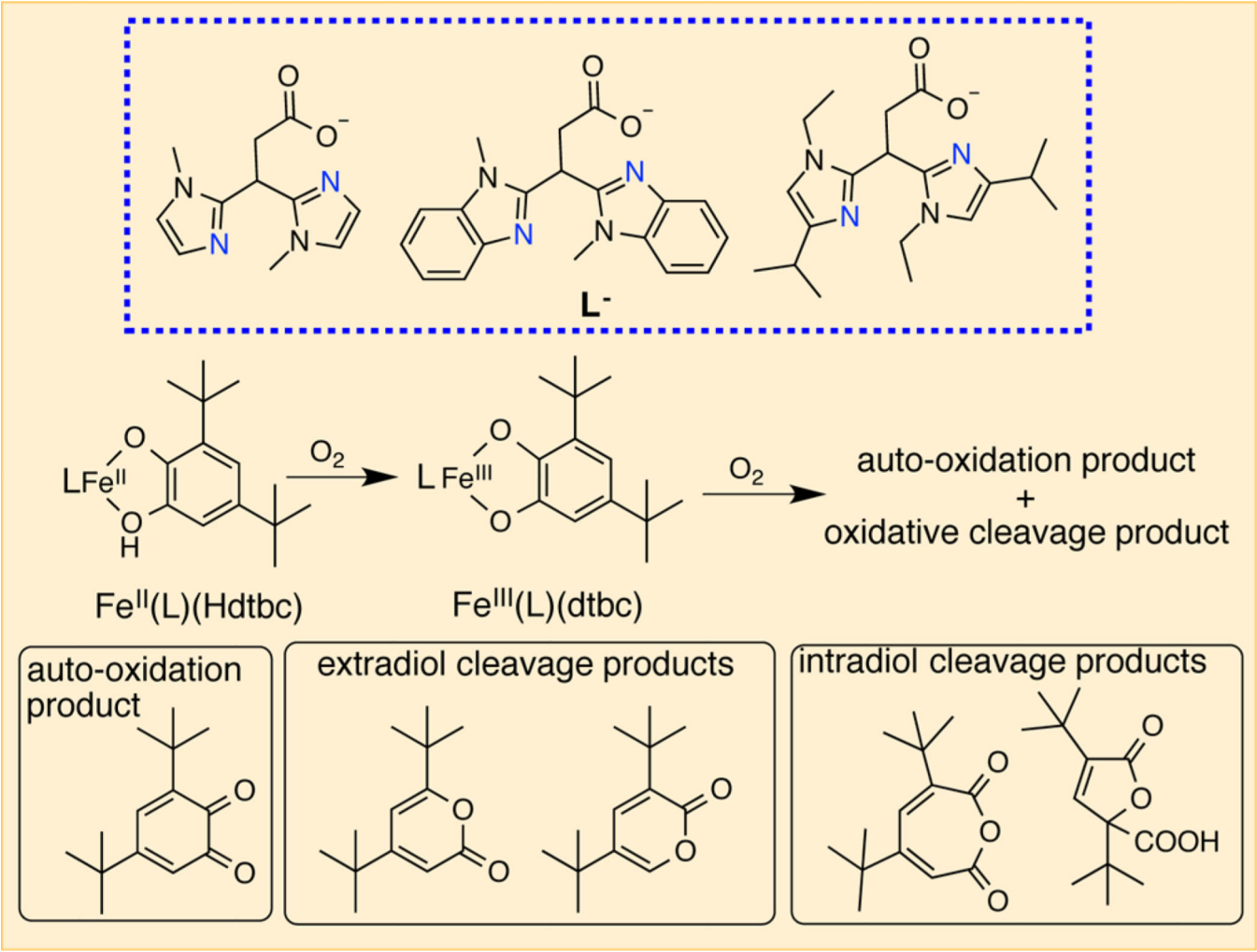


**Scheme 10.**

Ligands containg N,N,O Donor Atoms and Dioxygen Reaction Products for the $Fe^{II}$–Catecholate Complexes[a]

[a]Adapted with permission from ref 111. Copyright 2007 American Chemical Society.

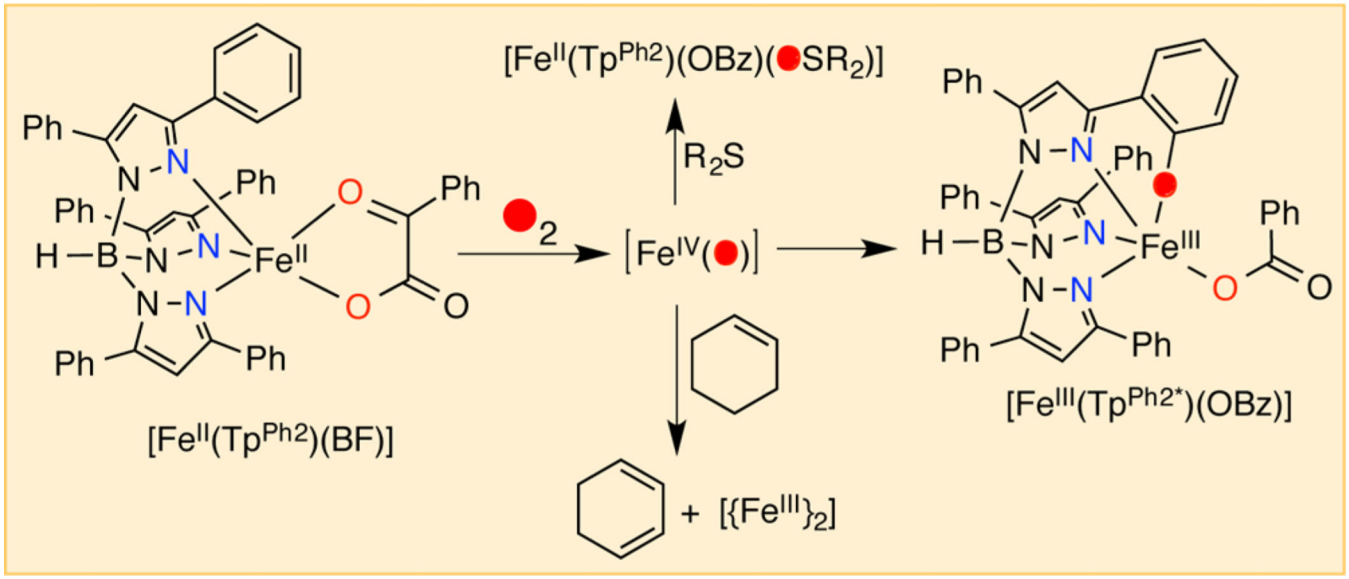


**Scheme 11.**

Interception of a Putative $Fe^{IV}(O)$ Intermediate, Generated from the Reaction of $[Fe^{II}(Tp^{Ph2})(BF)]$ and $O_2$[a]

[a]Reprinted with permission from ref 127. Copyright 2009 John Wiley & Sons, Inc.

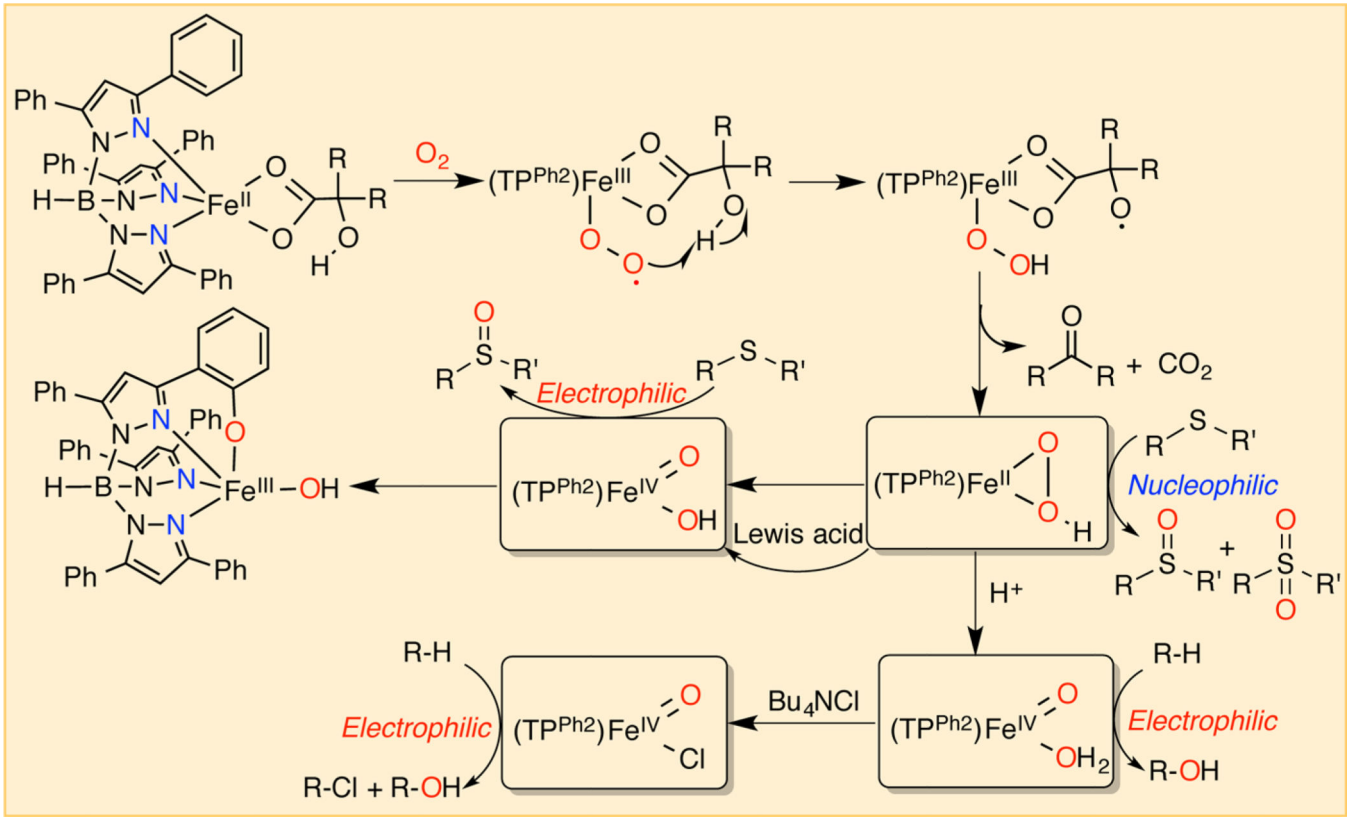


**Scheme 12.**

Reaction of [$Fe^{II}(Tp^{Ph2})$(benzilate)] with $O_2$ and the Interception of Various Active Oxidant Species[a]

[a]Adapted from refs 128 and 129. Copyright 2016 John Wiley & Sons, Inc., and Copyright 2015 John Wiley & Sons, Inc.

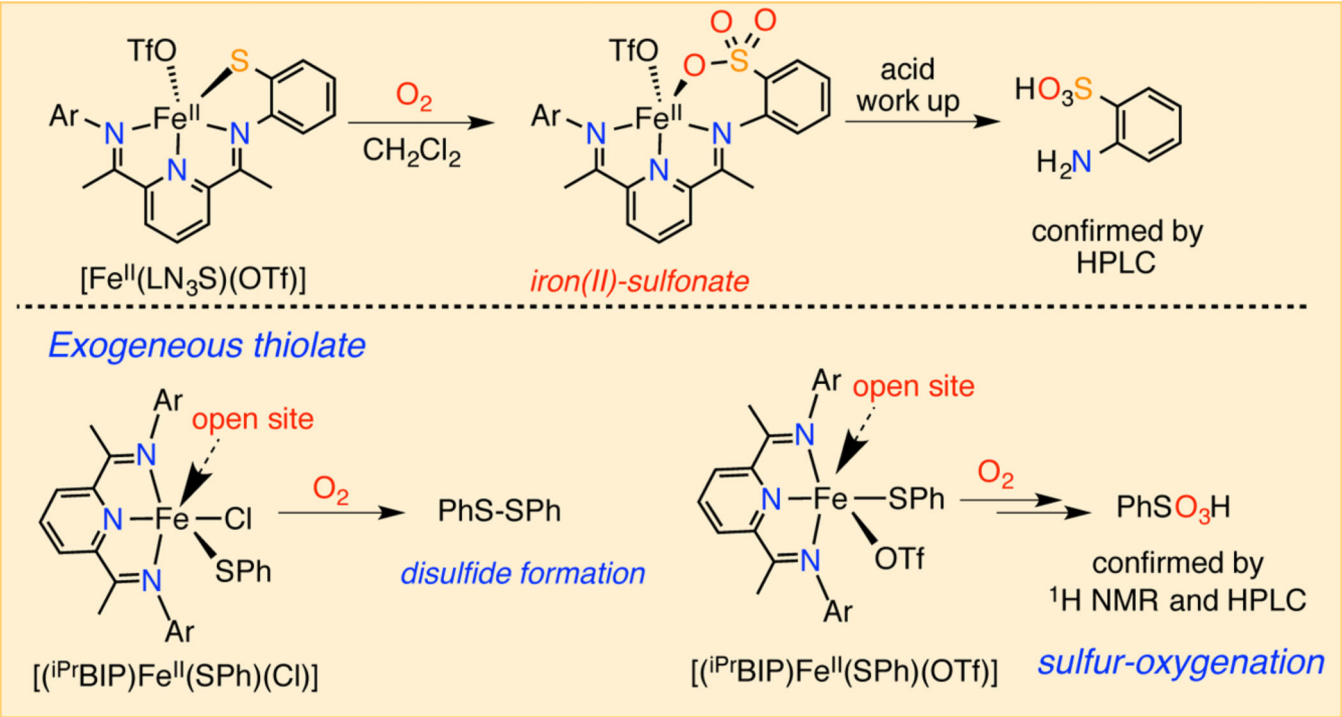


**Scheme 13.**

Examples of *S*-Oxygenation Reactions with Iron(II)–Thiolate Complexes and $O_2$[a]

[a]Adapted with permission from refs 140 and 141. Copyright 2010 American Chemical Society, and Copyright 2011 American Chemical Society.

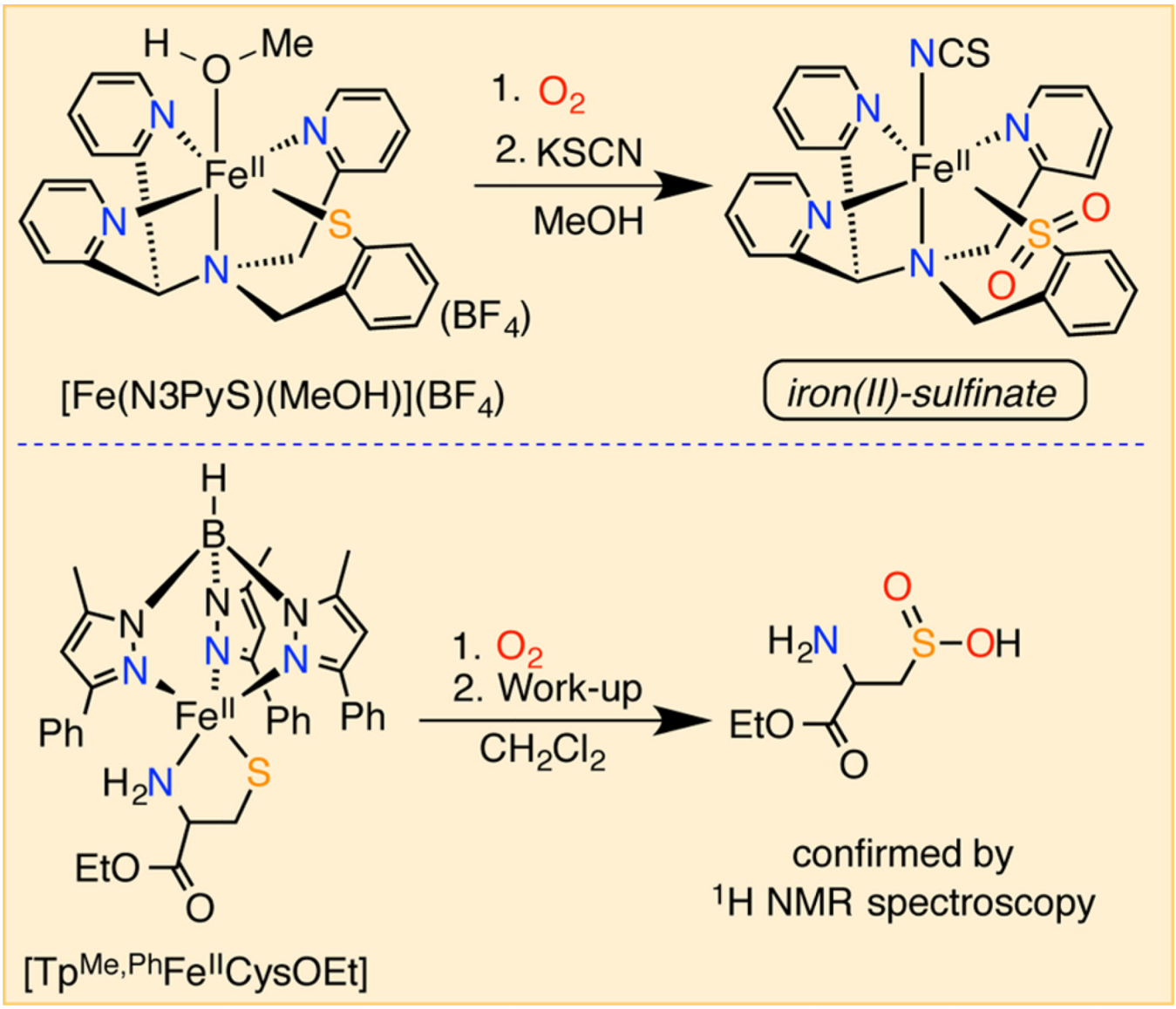


**Scheme 14.**

Double Oxygenation of Sulfur, Derived from the Reaction of an $Fe^{II}$–Thiolate Complex and $O_2$[a]

[a]Adapted with permission from refs 142 and 143. Copyright 2012 American Chemical Society, and Copyright 2012 John Wiley & Sons, Inc.

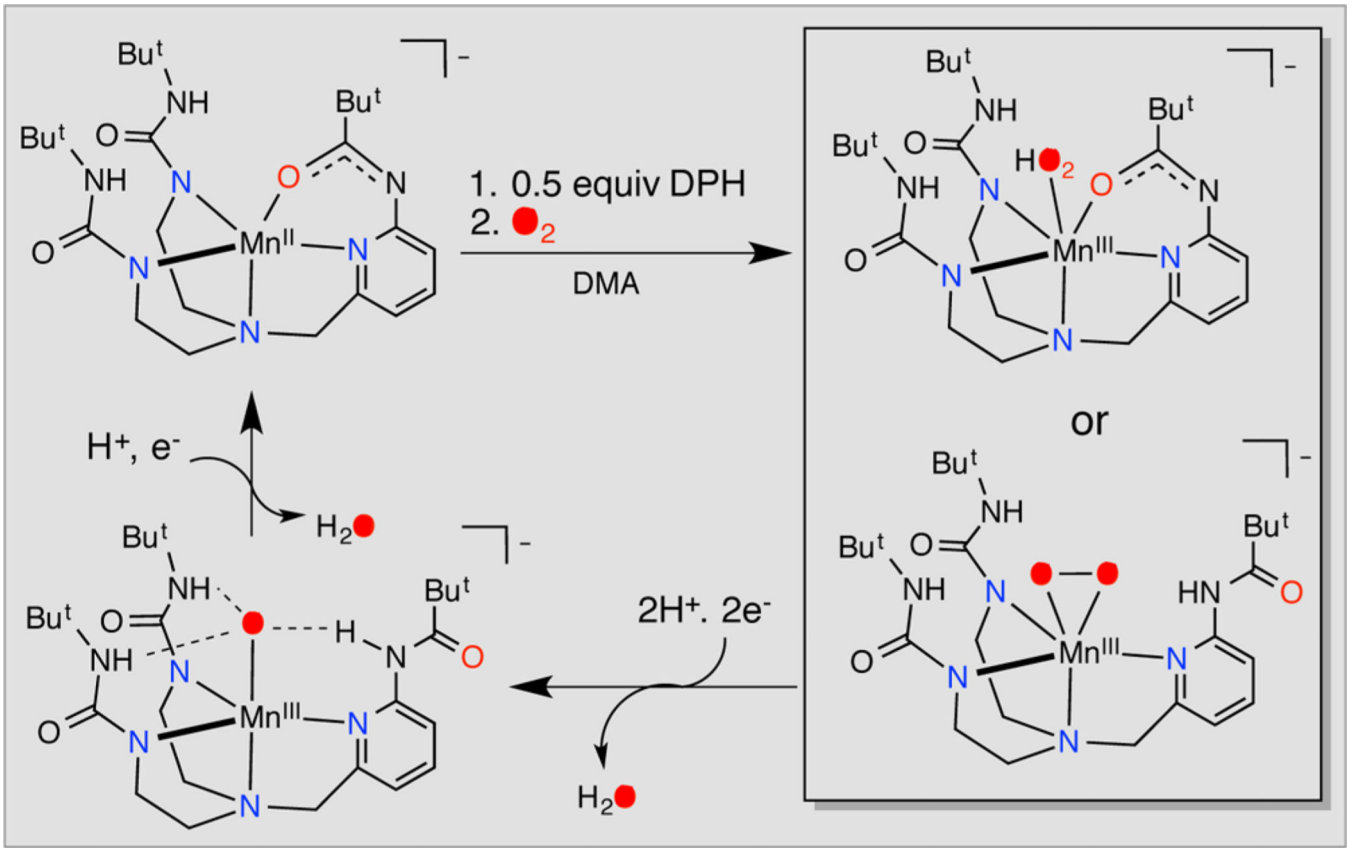


**Scheme 15.**

Catalytic Reduction of $O_2$ to $H_2O$ via the Intermediacy of $Mn^{III}$–Peroxo and $Mn^{III}$–O(H) Complexes[a]

[a]Adapted with permission from refs 154 and 155. Copyright 2008 American Chemical Society, and Copyright 2011 American Chemical Society.

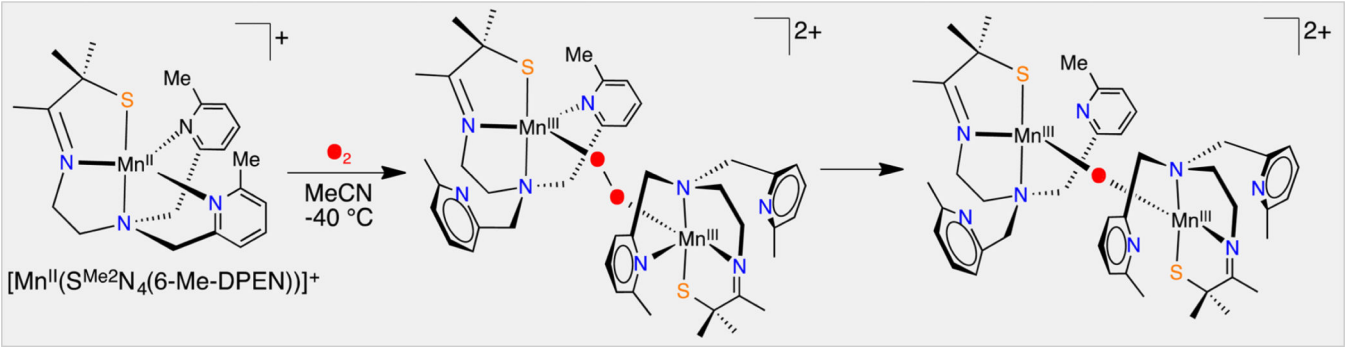


**Scheme 16.**

Low-Temperature Formation of a Peroxo-Bridged Dimanganese(III) Species from the Reaction of a $Mn^{II}$–Thiolate Complex + $O_2$, and Its Subsequent Conversion to a μ-Oxo-Bridged Dimeric Complex[a]

[a]Adapted with permission from ref 13. Copyright 2015 American Chemical Society.

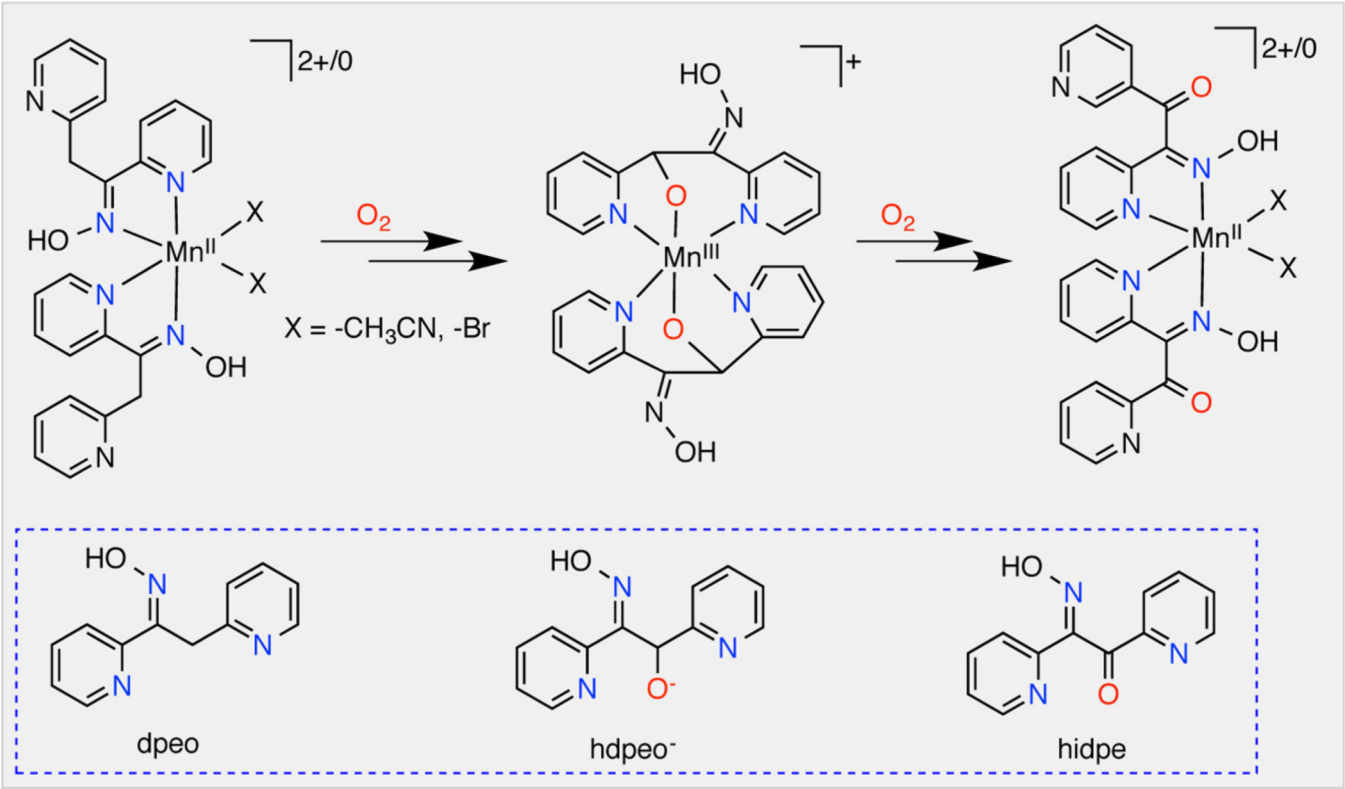


**Scheme 17.**

Stepwise Oxidation of Benzylic C–H Bonds Using $O_2$ by a $Mn^{II}$ Complex[a]

[a]Adapted with permission from ref 160. Copyright 2016 John Wiley & Sons, Inc.